TECHNICAL REPORT No. 54

FINITE ELEMENT SCHEMES FOR THE VERTICAL DISCRETIZATION OF THE ECMWF FORECAST MODEL USING LINEAR ELEMENTS

by

D.M. Burridge, J. Steppeler and R. Strüfing*

* Present affiliation:
Deutscher Wetterdienst
Offenbach/Main
Federal Republic of Germany

January 1986

Abstract

Two families of finite element schemes for vertical discretization are described for a sigma coordinate version of the ECMWF spectral model. The first, A-schemes, uses staggered node points which exploit the improved convergence that can be obtained in this way. The second family, B-schemes, are, unlike the A-schemes, formally energy conserving. Five versions of the B family (B0, B1, ... B4) are presented, each of which differs in the formulation of the upper (top) boundary element.

All schemes have been tested in a model with a coarse horizontal resolution, whilst schemes A, B0 and B2 have been evaluated in a T63 version of the 1983/84 ECMWF operational model. When compared with finite difference treatments, a systematic improvement in anomaly correlation of the height field forecasts was obtained; for the B schemes the average increase in the predictability was 2.5 hr and 6.5 hr, depending on the method.

In addition to forecast experiments, 50 day integrations with a T42 model were performed. The numerical schemes and the formulation of the upper boundary condition had considerable impact on these integrations. The finite element scheme showed less deviation of the time-averaged fields from the observations than the control run due to a better positioning of the troughs and ridges. The finite element scheme also improved the prediction of the time averaged anomaly field.

CONTENTS

1. INTRODUCTION

Even though computer power has increased enormously in the last 10 years the vertical resolution in primitive equation models of the atmosphere is quite low, 10 to 20 levels in the vertical being typical, and these are generally irregularly spaced to take account of the strong variation of atmospheric quantities in the vertical. Fig. 1 shows a schematic picture of the distribution of levels in a sigma coordinate version of the ECMWF spectral model which has the same resolution as the operational hybrid coordinate model over flat terrain. In comparison to the schemes used for horizontal discretization, the vertical discretization schemes in use in the majority of large-scale models of the atmosphere can be described, fairly, as rudimentary, based as they are on simple divided differences which provide second order accuracy at best; the irregularity of the level spacing reducing the local accuracy to first order. Large inaccuracies can be associated with boundaries.

Very few attempts have been made to employ the use of analytical functions which are continuously differentiable and defined globally; the two really potentially useful approaches (by Francis (1972) using Laguerre polynomials and by Machenhaur and Daley (1972) who used Legendre functions) have not lead to practical schemes for numerical models of the atmosphere.

In contrast to the global functional approaches of Francis, and Machenhaur and Daley, the use of local functional approaches based on a Galerkin implementation of finite elements has been fairly successful. The advantages of this approach are a better accuracy and, because of the reduced aliasing error of the Galerkin method, improved nonlinear

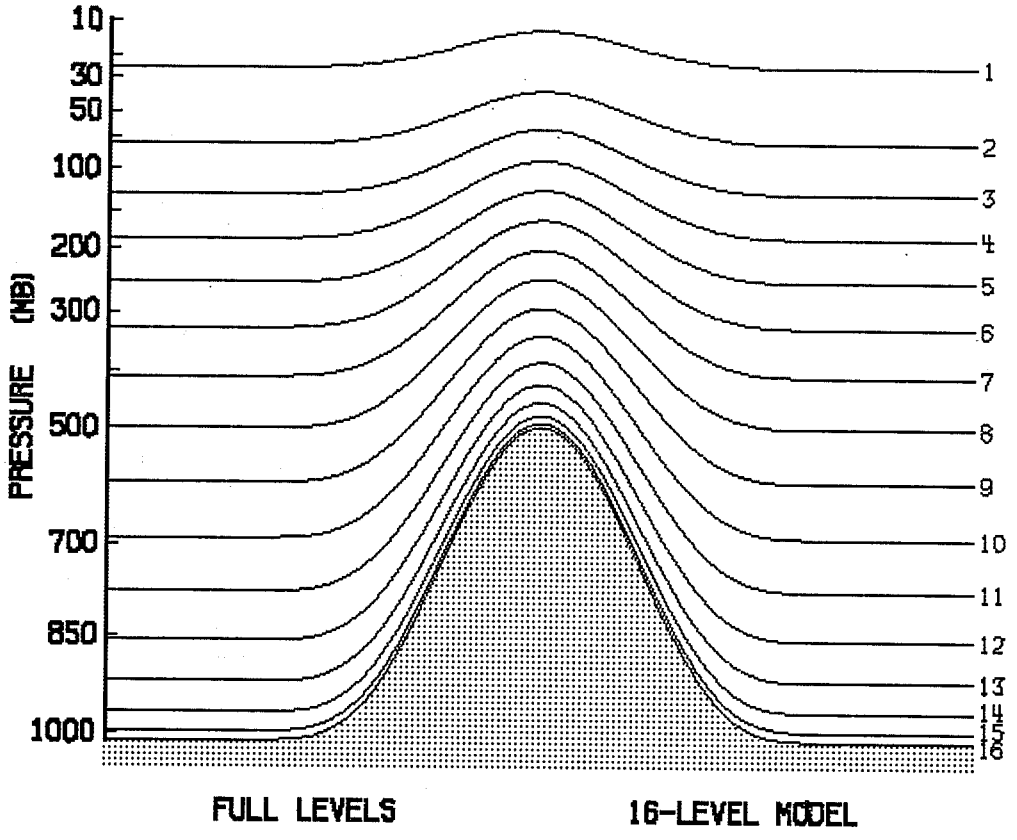

Fig. 1 Schematic picture of the full levels.

stability. Manton (1978) developed a finite element version of a one-dimensional boundary layer model. Also, a successful finite element formulation for the vertical discretization in sigma co-ordinate primitive equation models was described by Staniforth and Daley (1977), and a 36 hour forecast from real data demonstrated the viability of the method. The accuracy of their scheme was analysed by Béland et al. (1983) and the stability was investigated by Côté et al. (1983).

In this paper we consider two families of vertical finite element schemes. Family A is a natural evolution of ECMWF's basically second order finite difference scheme which is used for operational medium range forecasting. A main feature of this scheme is the use of a staggered system of node points which results in an increased accuracy for the vertical advection terms.

A second family, referred to as B-schemes, is formally energy conserving. Five B-schemes are introduced (B0, B1, B2, B3 and B4); these differ only in their formulation of the top element.

In Section 2 the various schemes are described, The results of various numerical experiments are presented in Section 3, and in Section 4 the 50 day integrations are described.

2. THE FINITE ELEMENT SCHEMES

The adiabatic part of the model is based on the primitive equations in σ-coordinates.

$$\dot{p}_s + \nabla.(p_s \underline{v}) + (p_s \dot{\sigma})_\sigma = 0$$

$$\dot{\underline{v}} + f\underline{k}x\underline{v} + \dot{\sigma}\underline{v}_\sigma + \underline{v}.\nabla\underline{v} + \nabla\phi + RT\nabla(\ln p_s) = 0$$

$$C_p p_s \dot{T} + C_p p_s \underline{v}.\nabla T + C_p p_s \dot{\sigma} T_\sigma - R\frac{T\omega}{\sigma} = 0 \qquad (1)$$

$$\dot{\sigma} = 0 \text{ for } \sigma = 0,1$$

$$\tilde{\phi}_\sigma = -\frac{RT}{\sigma}$$

$$\omega = p_s \dot{\sigma} + \sigma(\dot{p}_s + \underline{v}.\nabla p_s)$$

Field values are given for full model levels σ_ν. The operational ECMWF vertical discretization as described by Simmons and Strüfing (1981), uses half level values $\sigma_{\nu+\frac{1}{2}} = \frac{1}{2}(\sigma_\nu + \sigma_{\nu+1})$ to define the finite difference scheme.

The FE treatment is limited to the adiabatic part of the equations. The physical parameterisation, as well as the evaluation of the terms involving the humidity mixing ratio, is performed in node point space, as in the operational ECMWF model. In addition, the semi-implicit time integration scheme is taken over from the operational model without change.

A list of all the variables used in this paper is given in Table 1.

C_p: specific heat

$e^F_\nu(\sigma)$, $e^H_\nu(\sigma)$, $e^1_\nu(\sigma)$, $e^2_\nu(\sigma)$, $e^3_\nu(\sigma)$: basis functions belonging to the full and half levels, and various boundary options.

E^F, E^H, E^1, E^2, E^3 = function spaces generated by e^F_ν, e^H_ν, e^1_ν, e^2_ν and e^3_ν

f : Coriolis parameter

G^F, G^H, G^1, G^2, G^3 = Galerkin projections to spaces E^F, E^H, E^1, E^2 and E^3

M : mass matrix

M^{-1}: inverse of M

p_s: surface pressure

R : gas constant

T : temperature

$\underline{v}$: horizontal velocity

W : $\sigma\dot{p}_s+p_s\dot{\sigma}$

σ : vertical coordinate

$\dot{\sigma}$: vertical velocity

ϕ : geopotential

ϕ^H: geopotential projected to half level finite element space

Table 1 : List of symbols

2.1 Basic Galerkin equations

We consider here only the semi-discretization with respect to the vertical coordinate which leaves the horizontal variables undiscretized. Therefore our finite element schemes will involve just one space variable, and since we confine ourselves to the σ-system, we avoid the additional difficulties associated with the more general hybrid scheme introduced by Simmons and Strüfing (1981).

Consider a system of full level node points (see Fig. 1)

$$\sigma_\nu \ , \ \nu \in \{0, \ldots, NLEV+1\}$$

$$\text{with} \quad \sigma_o = 0 \quad \text{and} \quad \sigma_{NLEV} = 1 \tag{2}$$

We associate the following linear basis functions with these full level node points $\nu = 1, \ldots, NLEV$.

$$e_\nu^F(\sigma) = \begin{cases} \dfrac{\sigma_{\nu+1} - \sigma}{\sigma_{\nu+1} - \sigma_\nu} & \text{if } \sigma \in (\sigma_\nu, \sigma_{\nu+1}) \\ \dfrac{\sigma - \sigma_{\nu-1}}{\sigma_\nu - \sigma_{\nu-1}} & \text{if } \sigma \in (\sigma_{\nu-1}, \sigma_\nu) \\ 0 & \text{otherwise} \end{cases} \tag{3}$$

To formulate the different finite element schemes considered here, we need also a set of basis functions $e_\nu^H(\sigma)$ associated with the half levels $\sigma_{\nu+\frac{1}{2}}$. For schemes involving only one set of node points σ_ν, the index F of e in (3) will be dropped.

To formulate the different boundary treatments, we need three different versions ${}^1e_\nu(\sigma)$, ${}^2e_\nu(\sigma)$, ${}^3e_\nu(\sigma)$ of the full level basic functions $e_\nu^F(\sigma)$.

$${}^1e_\nu(\sigma) = e_\nu^F(\sigma)$$

$$\begin{cases} {}^2e_1(\sigma) = 1 & \text{for } \sigma \in (0, \sigma_1) \\ {}^2e_{NLEV}(\sigma) = 1 & \text{for } \sigma \in (\sigma_{NLEV}, 1) \\ {}^2e_\nu(\sigma) = e_\nu^F(\sigma) & \text{otherwise} \end{cases} \tag{4}$$

$$\begin{cases} {}^3e_1(\sigma) = 0 & \text{for } \sigma \in (0, \tilde{\sigma}) \\ {}^3e_\nu(\sigma) = e_\nu^F(\sigma) & \text{otherwise} \end{cases}$$

with $\tilde{\sigma}$ being a fixed small value of σ. Fig. 2 shows the different basis functions used in this study.

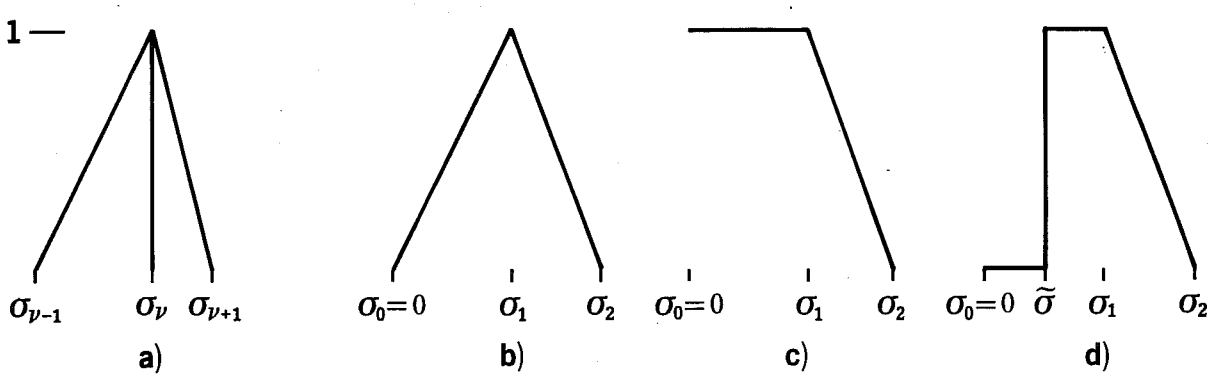

Fig. 2 The different basis functions used for the models. (a) ${}^{\mu}e_{\nu}(\sigma)$ for $\nu \neq \{1,\text{NLEV}\}$, (b) ${}^{1}e_{1}(\sigma)$, (c) ${}^{2}e_{1}(\sigma)$ and (d) ${}^{3}e_{1}(\sigma)$.

With any of the full level bases introduced above, we represent a field $\tilde{h}(\sigma)$ as

$$\tilde{h}(\sigma) = \sum_{\nu=1}^{\text{NLEV}} \tilde{h}_\nu \, e_\nu(\sigma) \tag{5}$$

The Galerkin procedure allows us to approximate the function $h(\sigma)$, not necessarily represented by an expansion such as (5), by a function $\tilde{h}(\sigma)$ of the class represented by (5). Functions like h may arise when forming the right-hand side of the prognostic equations with fields given by (5). The approximating equations are:

$$(e_\nu,\tilde{h}) = (e_\nu,h) \tag{6}$$

$$\text{with} \quad (e_\nu,h) = \int_0^1 e_\nu(\sigma)\, h(\sigma)\, d\sigma \tag{7}$$

Using (5), we can write (6) in the following form:

$$\sum_{\mu=1}^{\text{NLEV}} (e_\nu,e_\mu)\, \tilde{h}_\mu = (e_\nu,h)$$

$$\text{or} \quad M\underline{\tilde{h}} = \{(e_\nu,h)\} \tag{8}$$

$$\text{with} \quad M = \{(e_\nu,e_\mu)\} \text{ and } \underline{\tilde{h}} = \{h_\nu\}$$

With the linear elements of (3), M is a tri-diagonal matrix and, being diagonally dominant, can be inverted by Gaussian elimination without pivoting. Using the inverse matrix of M, we write (8) as:

$$\underline{\tilde{h}} = M^{-1} \{(e_\nu, h)\} \tag{9}$$

Equation (9), together with

$$\tilde{h}(\sigma) = \sum_\mu \tilde{h}_\mu \, e_\mu$$

defines an operation G, in which

$$Gh = \tilde{h} \qquad G : H \to E \tag{10}$$

with H being a space of rather general field functions $h(\sigma)$, and E being the space of approximating functions $\tilde{h}$ given by (5).

The Galerkin operator G provides an approximation Gh for every field $h(\sigma)$ from a rather general class of fields. The operator G has the following properties which will be used to provde energy conservation:

a) G is a linear operator

$$G(a_1 h_1 + a_2 h_2) = a_1 G h_1 + a_2 G h_2 \tag{11}$$

b) G is self-adjoint

$$(Gh_1, h_2) = (h_1, Gh_2) \tag{12}$$

with the scalar product (,) being defined by (7).

c) $$G^2 = G \text{ or } G(Gh) = Gh \tag{13}$$

Equation (13) implies that G does not change fields which are already in the class of approximating functions. Considering H as a Hilbert space under the scalar product defined by (7), (11)-(13) mean that the Galerkin operator G is a projection operator.

In the following we will use the bases ${}^1e_\nu$, ${}^2e_\nu$, ${}^3e_\nu$ defined in (4). The corresponding Galerkin operations will be denoted by G^1, G^2, G^3; the operation G^3 will be necessary both for full and half levels of σ, the corresponding basis-functions being defined in (3). We denote the corresponding Galerkin operations as G^F and G^H.

2.2 Description of the A-family

In this section we use the ${}^3e_\nu$-basis defined in (4), and the index 3 will be dropped. The basic fields will be represented by full level nodes, the corresponding basis being denoted as e^F_ν. For some intermediate steps the half level representation will be used with basis denoted by e^H_ν. The spaces of approximating functions according to (5) are denoted by E^F and E^H, and the corresponding Galerkin projections are denoted by G^F and G^H.

We write the continuity equation as

$$\frac{\partial W}{\partial \sigma} + D = 0 \qquad (15)$$

with $W = \sigma \dot{p}_s + p_s \dot{\sigma}$ and $D = \nabla.(p_s \underline{v})$.

Since $\underline{v}$ has full level nodes, D is in the space E^F, and we assume that $\dot{\sigma}$, and hence W, has half level nodal points.

$$D = \sum_\nu D_\nu \, e^F_\nu \qquad \varepsilon \; E^F$$

(15)

$$W^H = \sum_\nu W_{\nu+\frac{1}{2}} \, e^H_\nu \qquad \varepsilon \; E^H$$

The $\dot{\sigma}$ belonging to W^H, according to (14), is denoted as $\dot{\sigma}^H$.

For geopotential, which also has half level nodes, we have

$$\phi^H = \sum_\nu \phi_{\nu+\frac{1}{2}} e^H_\nu \tag{16}$$

with the equation for the $\phi_{\nu+\frac{1}{2}}$ being

$$(e^F_\nu, (\frac{\partial \Phi}{\partial \sigma} + \frac{RT}{\sigma})) = 0 \tag{17}$$

In this equation, T is given at the full levels. Since $\phi_{NLEV+\frac{1}{2}} = \phi_s$, with ϕ_s being the surface geopotential, (17) has the correct number of equations.

The approximations made in deriving $\dot{\sigma}$ and ϕ imply the form of the ω-term and the vertical advection term - see Appendix 1 for further details.

The other terms of the prognostic equations are represented by straight forward Galerkin projections, and we write the prognostic equations for $\underline{v}$ and T as

$$\begin{aligned}\dot{\underline{v}} + f\underline{k}\times\underline{v} + G^F(\underline{v}\cdot\nabla\underline{v}) + G^F[(\dot{\sigma}^H G^H\underline{v})_\sigma + \underline{v}\,(\frac{\dot{p}_s}{p_s} + \frac{\nabla\cdot(p_s\underline{v})}{p_s})] \\ + G^F\nabla\phi^H + RT\nabla \ell n p_s = 0\end{aligned} \tag{18}$$

$$\begin{aligned}C_p p_s \dot{T} + C_p p_s G^H\underline{v}\cdot\nabla T + G^F[(\dot{\sigma}^H G^H T)_\sigma + T_s(\frac{\dot{p}_s}{p} + \frac{\nabla\cdot(p_s\underline{v})}{s\ p}) \\ + G^F[(\phi^H W^H)_\sigma + \phi^H D + RT\underline{v}\cdot\nabla p_s] = 0\end{aligned}$$

2.3 Formulation of the B-family

A general form of energy conserving Galerkin discretizations of the primitive equations is:

$$\dot{p}_s + \nabla.(p_s \underline{v}) + (p_s \dot{\sigma})_\sigma = 0$$

$$\dot{\underline{v}} + f\underline{k}x\underline{v} + G_a(\dot{\sigma}\, \underline{v}_\sigma) + G_a(\underline{v}.\nabla\underline{v}) + G_a\nabla\tilde{\phi} + RG_a\tilde{\tilde{T}}\nabla \ell n p_s = 0$$

$$C_{pp_s}\dot{T} + C_{pp_s}G_b(\underline{v}\cdot\nabla T) + C_{pp_s}G_b(\dot{\sigma}\, T_\sigma)$$

$$- RG_b\left(\frac{\tilde{T}\omega_1}{\sigma}\right) - RG_b\left(\frac{\tilde{\tilde{T}}\omega_2}{\sigma}\right) = 0 \qquad (19)$$

$$\dot{\sigma} = 0 \quad \text{for } \sigma = 0,1$$

$$\tilde{\phi}_\sigma = -\frac{R\tilde{T}}{\sigma}$$

$$\omega = \omega_1 + \omega_2$$

$$\omega_1 = p_s\,\dot{\sigma} + \sigma\,\dot{p}_s \text{ and } \omega_2 = \sigma\underline{v}.\nabla p_s$$

It is assumed that $\underline{v}$ is represented in the approximation space E_a belonging to G_a, and T is represented by the approximation space E_b belonging to G_b.

We must require:

$$1 \in E_b \qquad (20)$$

This is satisfied by the space E_2 defined in Section 2.1, but not by E_1. Therefore we are led to use the ${}^2e_\nu$ representation for the temperature field.

In (19), $\tilde{T}$ and $\tilde{\tilde{T}}$ can be chosen independently. However, the relation between $\tilde{T}$, $\tilde{\tilde{T}}$ and T can be obtained by a Galerkin operation, but this is not essential. In the present study we choose $\tilde{T}=\tilde{\tilde{T}}=T$ for $\sigma<\sigma_1$. Only in the top σ interval will different formulations for $\tilde{T}$ and $\tilde{\tilde{T}}$ be used, as explained in Section 2.4.

Equation (19) gives a rather general form of an energy conserving Galerkin discretization of the primitive equations. In this form it is valid for high order finite element schemes or other Galerkin methods, for example those based on Chebycheff polynomials.

If in addition we choose $\tilde{T} = \tilde{\tilde{T}} = T$, then we obtain a straightforward Galerkin dicretization. Since energy is essentially a second order moment in σ-coordinates, the P_s factor being independent of σ, then (19) describes a formally energy conserving scheme (Jespersen, 1974 and Cliffe, 1981). The proof of energy conservation is given in Appendix 2.

It should be noted, that the diagnostic equations in (19) contain no approximation operators at all. This means that $\dot{\sigma}$, ϕ and ω must be obtained by exact integration using the linear spline assumption for the other fields. For $\dot{\sigma}$ and ω this is achieved by representing them as quadratic splines.

The basic B-family scheme, scheme B0, is defined by

$$G_a = G_1 \ , \ G_b = G_2 \ , \ \tilde{T} = T \qquad (21)$$

Other schemes, called B1, B2, B3 and B4 will be introduced which differ from B0 only in their formulation of the top element.

2.4 Definition of top element formulations for the B-schemes

To illustrate a deficiency of the B0-scheme near the boundary, Fig. 3a gives the Φ field resulting from an exact integration. Linear elements are assumed for the temperature representation, with the temperature element being constant in the top interval $(0,\sigma_1)$. The nodal values of the temperature are those of a randomly chosen gridpoint from an ECMWF analysis. Because of the interpolation assumption in the top interval, a logarithmic singularity in Φ appears.

Fig. 3b shows the Galerkin projection of this field on the test-function space used for the representation of the velocity field in the B0 scheme. Noise is generated near the top of the model. This effect is almost certainly physically unrealistic, particularly since it is dependent on the choices of the interpolation for the temperature and velocity fields in the top interval.

It should be noted that the interpolation of the temperature field leading to Fig. 3a imposes the T-gradient at $\sigma=\sigma_1$ on the interval$(0,\sigma_1)$. Therefore the numerical bias shown in Figs. 3a,b will appear in the same way for the approximation of $\nabla\phi$.

We have used two principles to guide our choice of the top element function:

(a) For appropriate amplitudes, the chosen functions for the top element should allow geostrophic balance <u>throughout</u> the top interval $(0,\sigma_1)$.

(b) The geostrophic wind should remain finite for $\sigma\to 0$.

Condition (b) is equivalent to the condition:-

$$\nabla T \to 0 \text{ for } \sigma \to 0. \qquad (22)$$

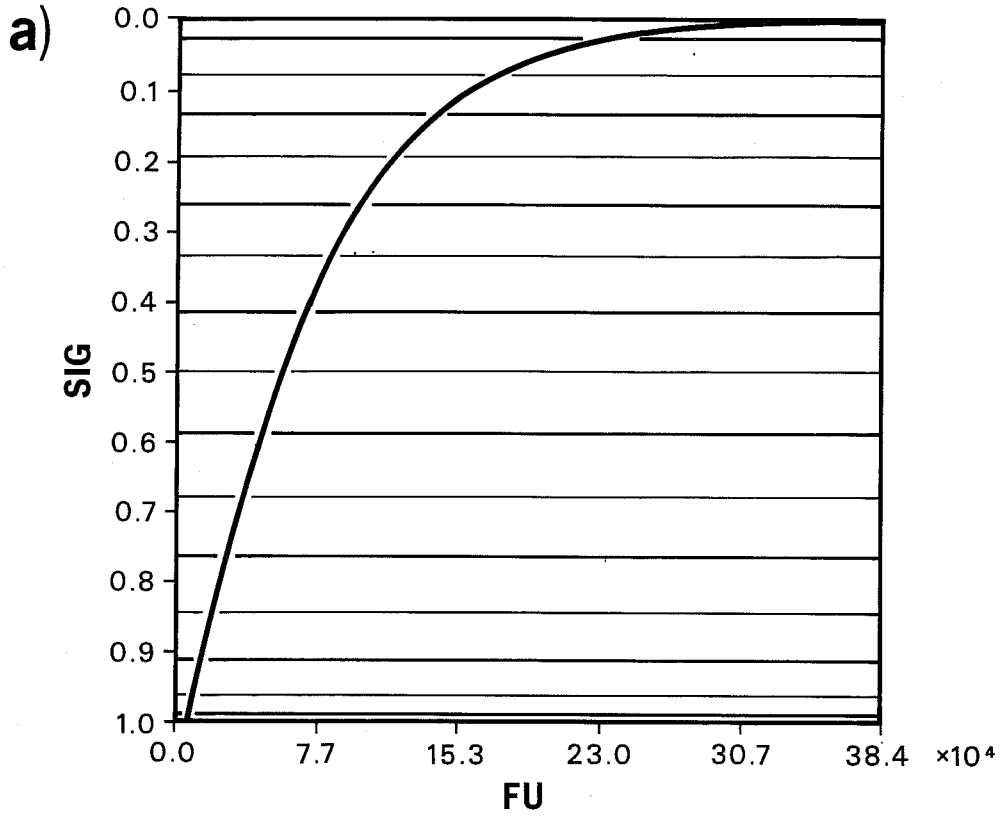

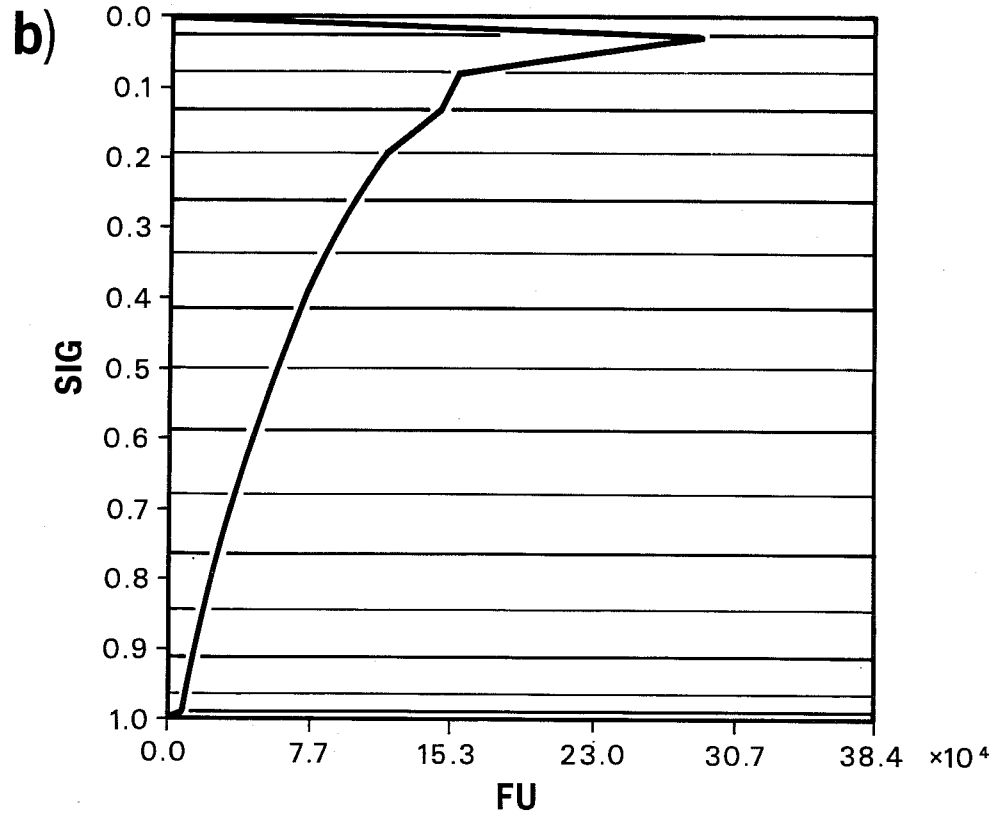

Fig. 3 (a) Exact integration of ϕ and (b) the projection of ϕ to $\underline{v}$ elements in the B0 scheme.

In the model of Machenhauer and Daley (1972), (22) was used as a boundary condition when using Legendre polynomials for vertical discretization. With the finite element scheme, it would formally be possible to satisfy condition (a) whilst violating condition (b). If the elements for the T-representation approach some constant value for $\sigma \to 0$, the appropriate elements for the velocity fields would contain a logarithmic singularity at $\sigma=0$. Since all powers of $\log(\sigma)$ are integrable, the corresponding finite element scheme is well defined. We would, however, expect problems with the CFL-criterion for the upper levels. In this study, this possibility is not followed further.

We will not necessarily assume that for every state of the temperature field we find a matching velocity field. For example one possibility is to provide a temperature amplitude for $\sigma=0$ and leave it to the model to produce condition (a). The elements for the velocity fields will then be chosen to allow matching only for cases when (22) is satisfied.

In the following we denote the basis functions used for the representation of $\underline{v}$ and T in (19) as e^{v}_{ν} and e^{T}_{ν}.

Method B1

$$G^a = G^b = G^2\, T \tag{23}$$

$$\tilde{T} = \tilde{\tilde{T}} = T$$

Method B2

$$G^a = G^b = G^2\, T$$

$$\tilde{T} = \tilde{\tilde{T}} = \frac{T_1}{\sigma_1}\,\sigma \qquad \text{for } \sigma \in (0,\sigma_1) \tag{24}$$

$$\tilde{T} = \tilde{\tilde{T}} = T \qquad \text{otherwise}$$

Method B3

A rather good consistency of the T and v elements can be achieved by introducing a top amplitude T_o for $\sigma=0$; this then becomes the same as the B2 scheme with $\sigma_1=0$. We should expect that grad T_o approaches zero during the forecast.

The integrations with boundary treatment B2 were somewhat noisy at the top most level; this noise was geographically related to the orography field. However, in the course of ten day integrations, this noise did not contaminate the other levels. It was caused by the B2-scheme not allowing the representation of an isothermal atmosphere and appeared in all integrations.

Method B4

Scheme B4 has evolved from B2 in order to solve this noise problem. A test integration gave similar results for schemes B2 and B4, except for the top level.

The scheme is as B2, but with $\tilde{\tilde{T}}=T$ everywhere.

In the integration reported in Section 4, this scheme was used in the simplified form:

$$R\,G_b\left(\frac{\tilde{\tilde{T}}\,W_2}{\sigma}\right) \Rightarrow R\,G_b\left(\frac{T\,W_2}{\sigma}\right) \qquad (25)$$

$$R\,G_a\,\tilde{\tilde{T}}\ln p_s \Rightarrow R\,G_a\,\tilde{T}\ln p_s$$

This latter form implies a deviation from energy conservation for the top level.

3. FORECAST EXPERIMENTS

3.1 The numerical experimentation

The main numerical experimentation was based on a set of 6 cases; the initial dates of these are given in Table 2. Control runs were provided by a sigma coordinate version of the 1983/84 ECMWF operational spectral model, as described by Simmons and Strüfing (1981). This model has a triangular truncation for the horizontal representation, and the main comparisons were carried out with a T63 model (triangular truncation at total horizontal wave number 63). In addition many preliminary experiments were performed at reduced resolution of T21 and for the A scheme some extra T63 computations were carried out from dates not listed in Table 2. The vertical resolution is illustrated in Fig. 1.

Experiment No.	Date
1	10.01.84
2	01.01.84
3	25.12.83
4	16.08.83
5	07.04.83
6	23.08.83

Table 2 The initial dates of the test experiments the B-schemes.

The objective comparison of the different schemes is based mainly on a predictability measure. For this study, our measure of the predictability of a meteorological element is the number of days into the forecast before an anomaly correlation threshold (usually 60%) is first reached.

The largest improvements obtained with the A-scheme was for the forecast from 24.1.82. Fig. 4 shows the anomaly correlations of height for two T63 integrations - control and scheme A. For this case the use of scheme A produces a 6 hour increase in predictability over that of the control. Because of its lack of energy conservation, most of the experimentation was carried out with the B-schemes.

As a preliminary test of the different B-schemes, an initial set of experiments was performed with T21 horizontal truncation. Although there was little to choose between the various B-schemes at this resolution, they were all slightly better than the control. However, some of these schemes needed a rather small timestep in order to be stable. The required timesteps were investigated experimentally and are given in Table 3.

Method	Timestep
ECMWF-operational	45 min
B0	45 min
B1	15 min
B2	45 min
B3	10 min

Table 3: Stability timesteps for T21 model runs using different treatments of the vertical coordinate

For tests with a higher resolution, schemes B0 and B2 were chosen and experiments were carried out from the dates given in Table 2. The time step for most of these forecasts was 20 minutes. However, some of the integrations with the B2-scheme turned out to be unstable; stable results were obtained with a 15 minute timestep.

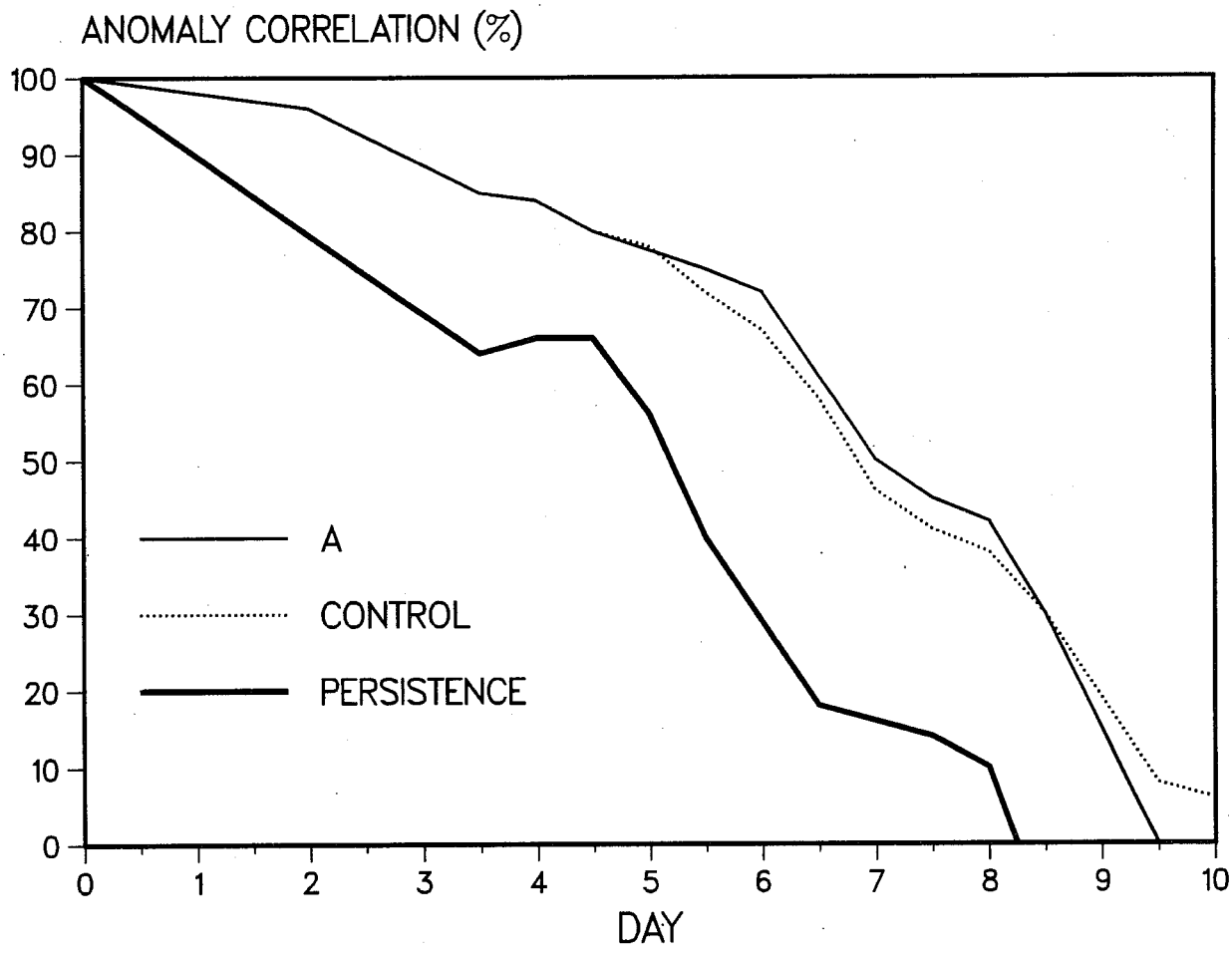

Fig. 4 Mean 200-1000 mb anomaly correlation of height (wavenumbers 1-3) for scheme A (initial date 24 December 1984).

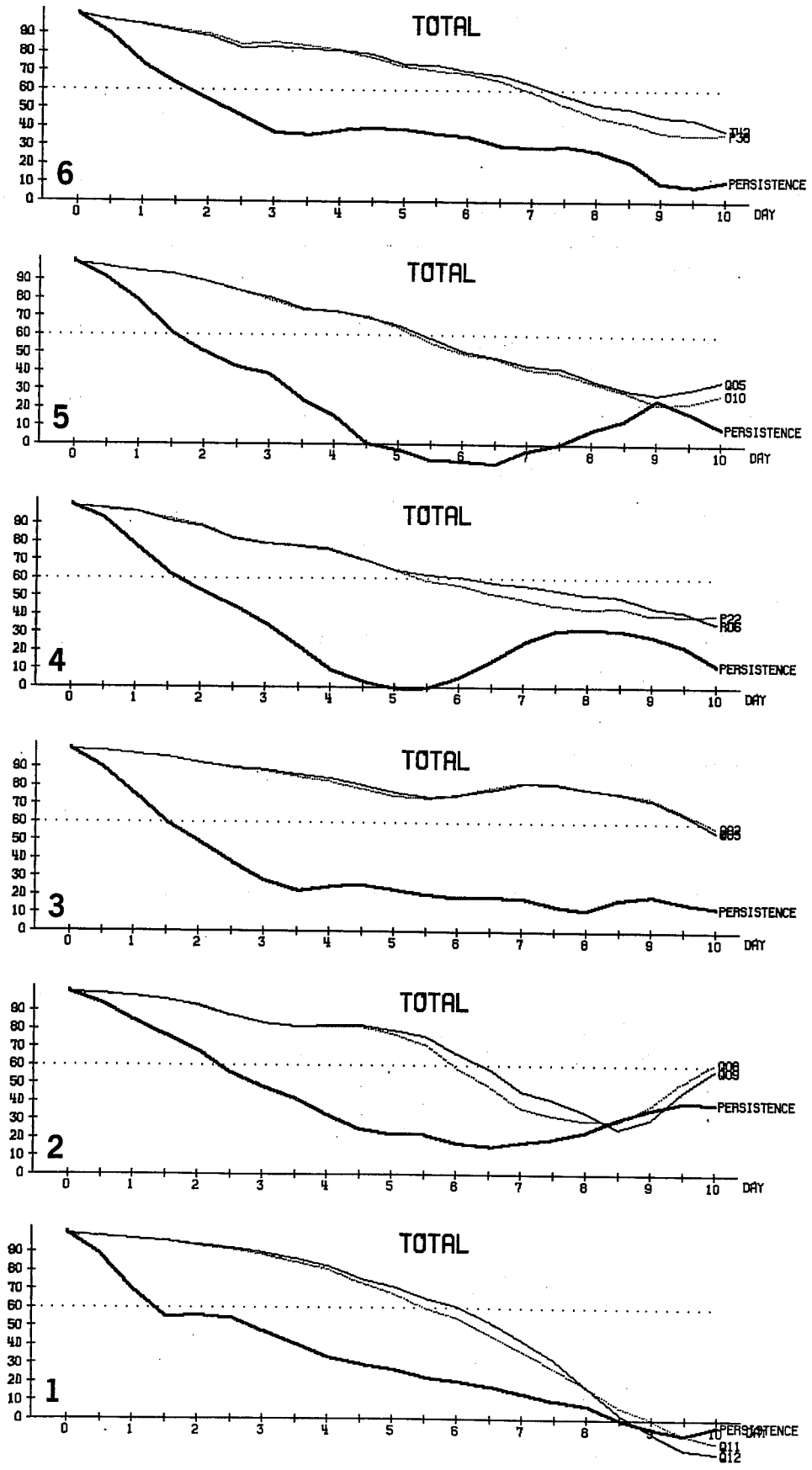

Fig. 5 Anomaly correlation of the 1000 mb heights for 6 cases using the B2 scheme (dates indicated in Table 2). Thick line - persistence, dashed line - control thin line - scheme B2.

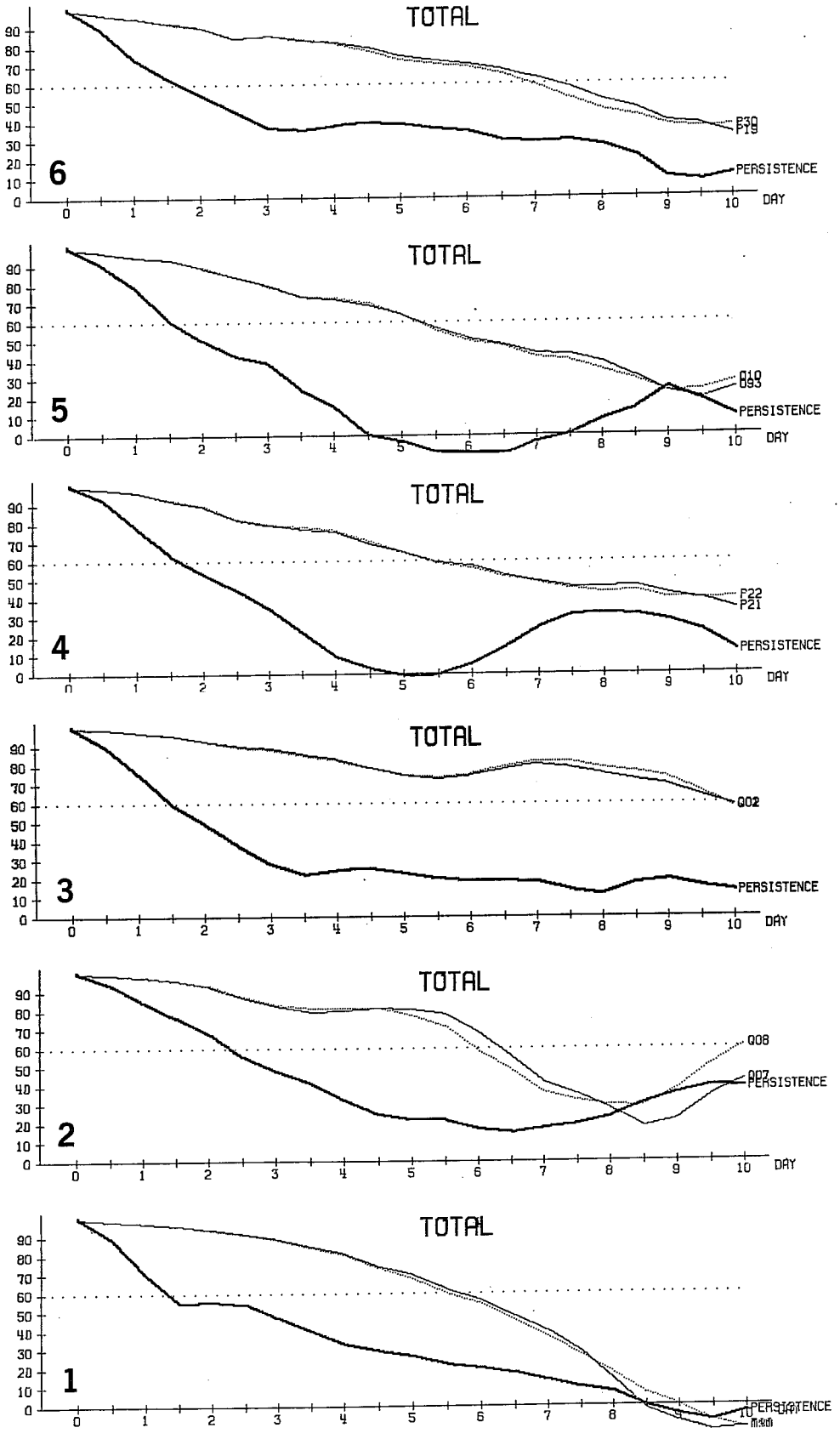

Fig. 6 Mean 1000 mb anomaly correlation for 6 cases using the BO scheme. Lines labelled as in Fig. 5.

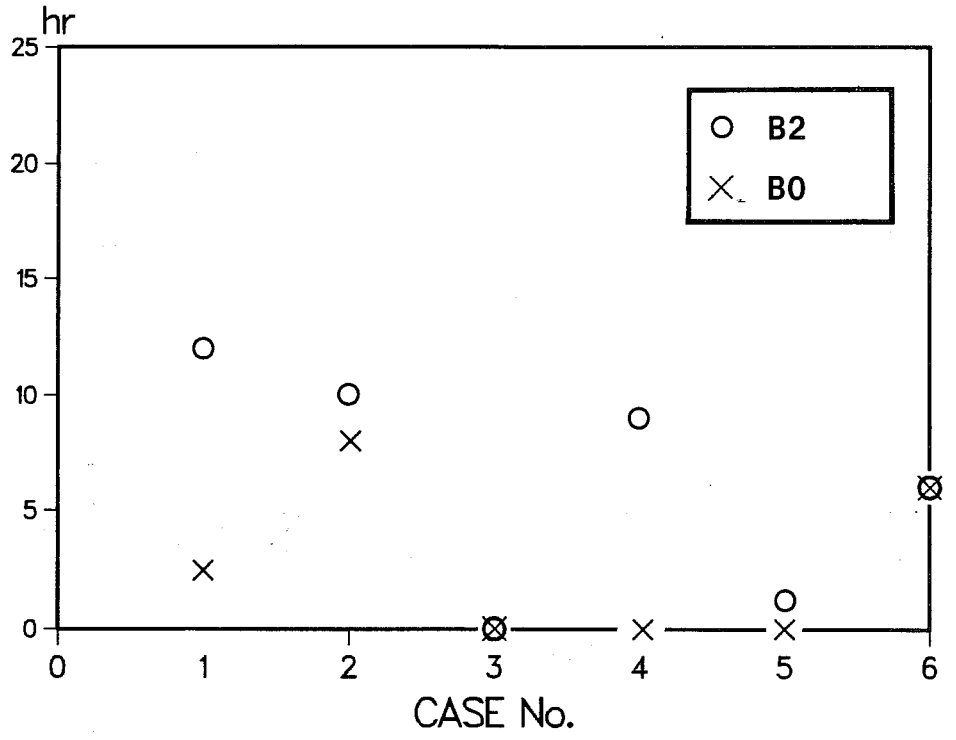

Fig. 7 Increase in predictability at the 60% anomaly correlation threshold for scheme B0 and B2 compared with the control.

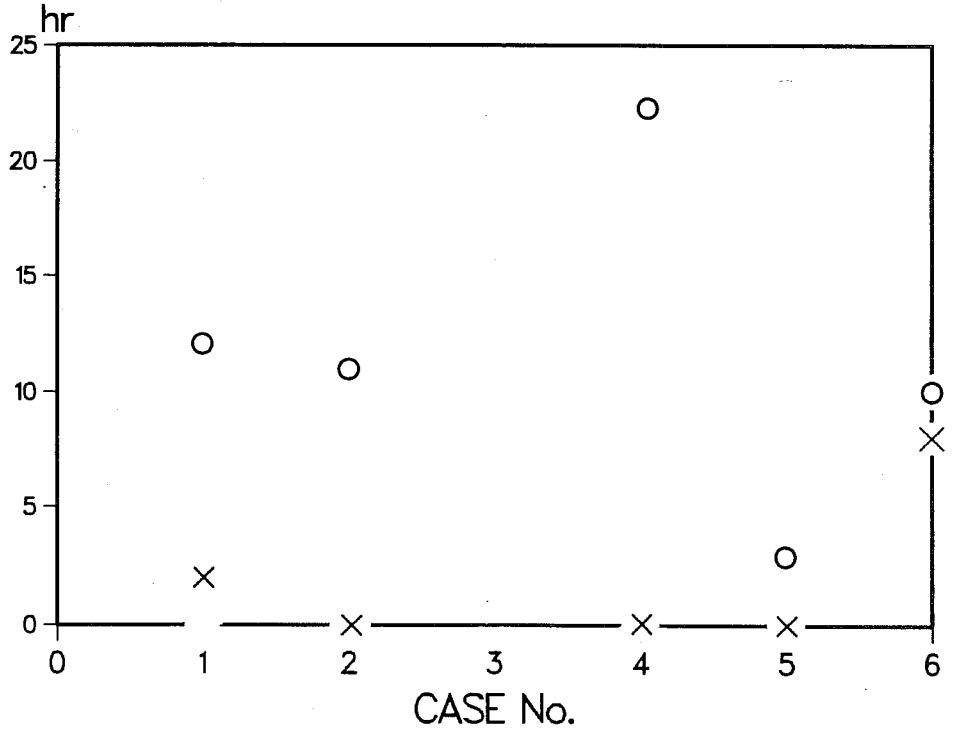

Fig. 8 As Fig. 7, but for the 50% threshold.

3.2 Results from forecast experiments with the T63 model

Fig. 5 shows the anomaly correlations of 1000 mb height for the B2-scheme. Four cases show an appreciable improvement over the control in the correlation which ranges between 5 and 10% at about day 6; cases 3 and 5 are neutral. Fig. 6 shows the corresponding results for the B0 scheme. The improvements for the B0-schemes are generally smaller than for the B2-scheme. However, in all cases the B0 scheme produced an improvement over the control or was neutral.

Figs. 7 and 8 gives the increase in predictability for schemes B2 and B0 for the 60% and 50% thresholds respectively. The average increase of predictability obtained from Fig. 7 is 6.5 hr for the B2 scheme and 2.5 hr for the B0 scheme. For the 50% correlation threshold the values are 11 hr and 3.5 hr.

These results suggest that the formulation of the top boundary elements might have a considerable influence on the forecast scores. This finding is consistent with the results obtained by Beaudoin et al. (1980).

In the southern hemisphere the finite element forecasts are a little better than those from the control, however the largest improvements occur at very low levels of skill.

In spite of the improvement in the objective scores, for the cases evaluated so far there appears to be little synoptic difference between finite element and finite difference forecasts. This is probably due to the fact that the finite element treatment has improved the largest scales only. Therefore we give here only a few examples to illustrate the synoptic differences due to difference numerical treatments.

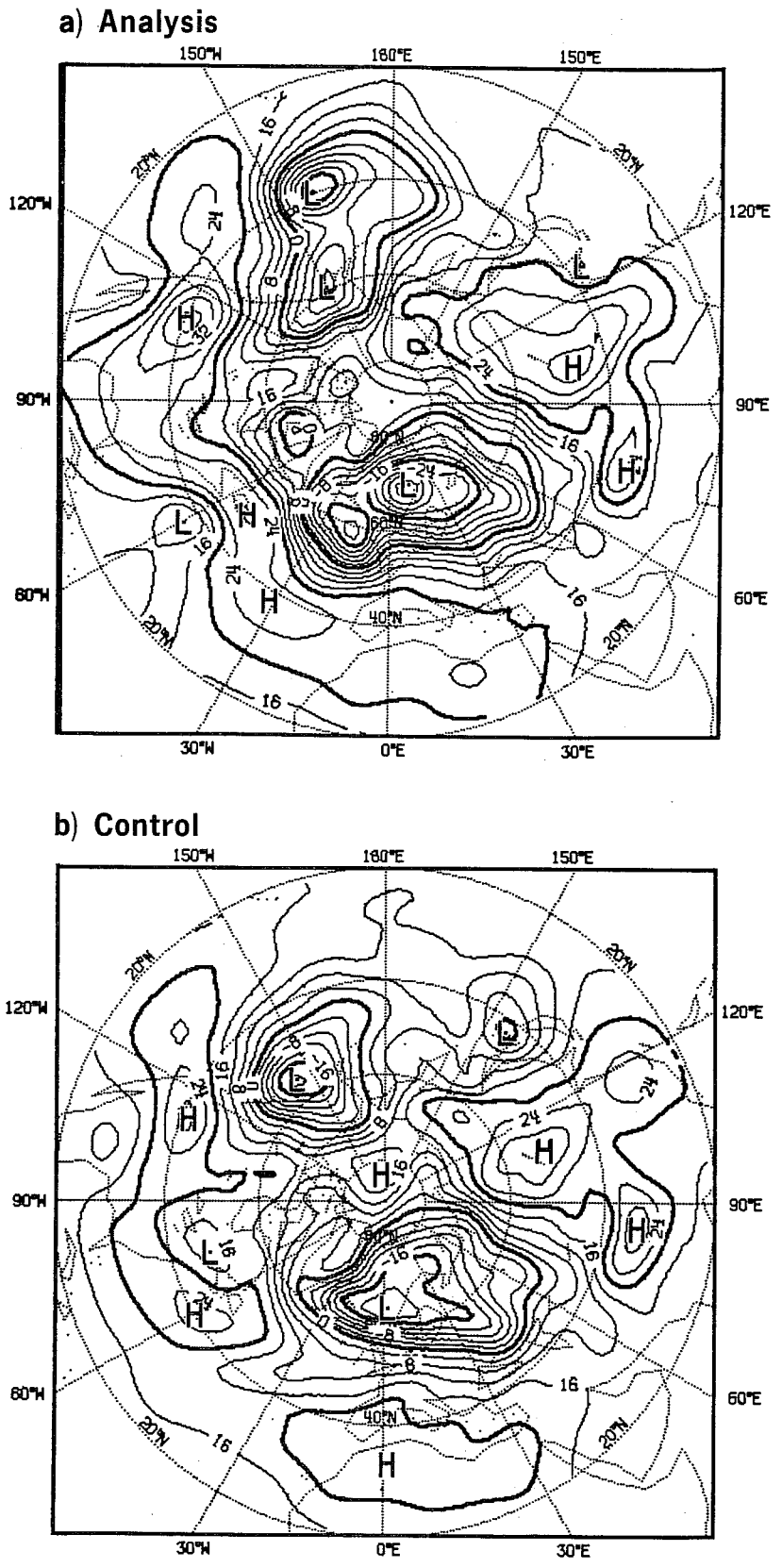

Fig. 9 1000 mb height fields for a 6 day forecast from 25 December 1983 for (a) verifying analysis, (b) control, (c) scheme B2 and (d) scheme B0. Contour interval 4 dkm.

c) Scheme B2

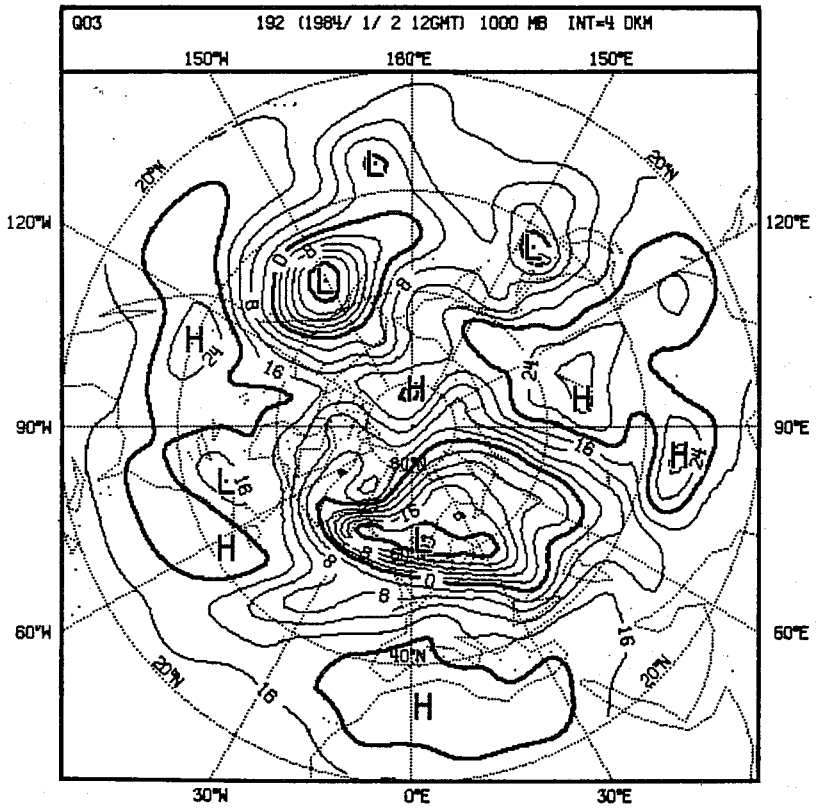

d) Scheme B0

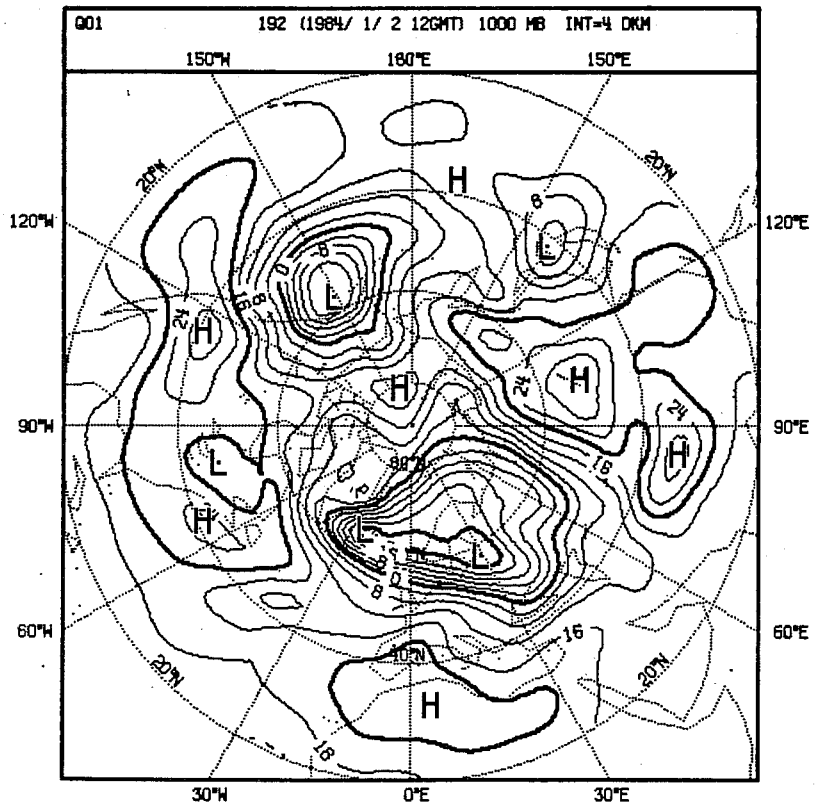

Fig. 9 (Contd.)

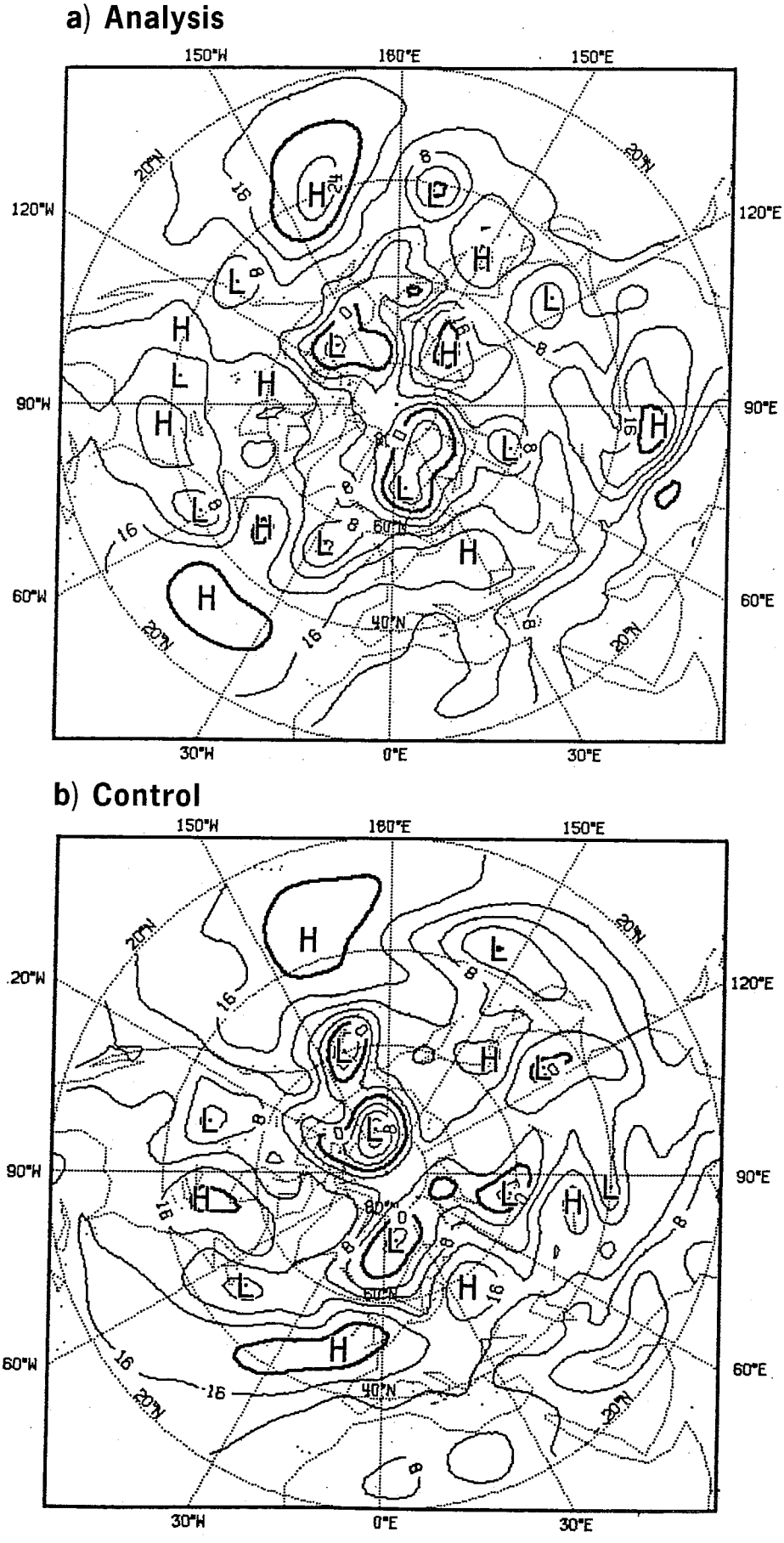

Fig. 10 D+7 for forecast form 23.8.83, 1000 mb height field. a) Analysis, b) control, c) scheme B2.

c) Scheme B2

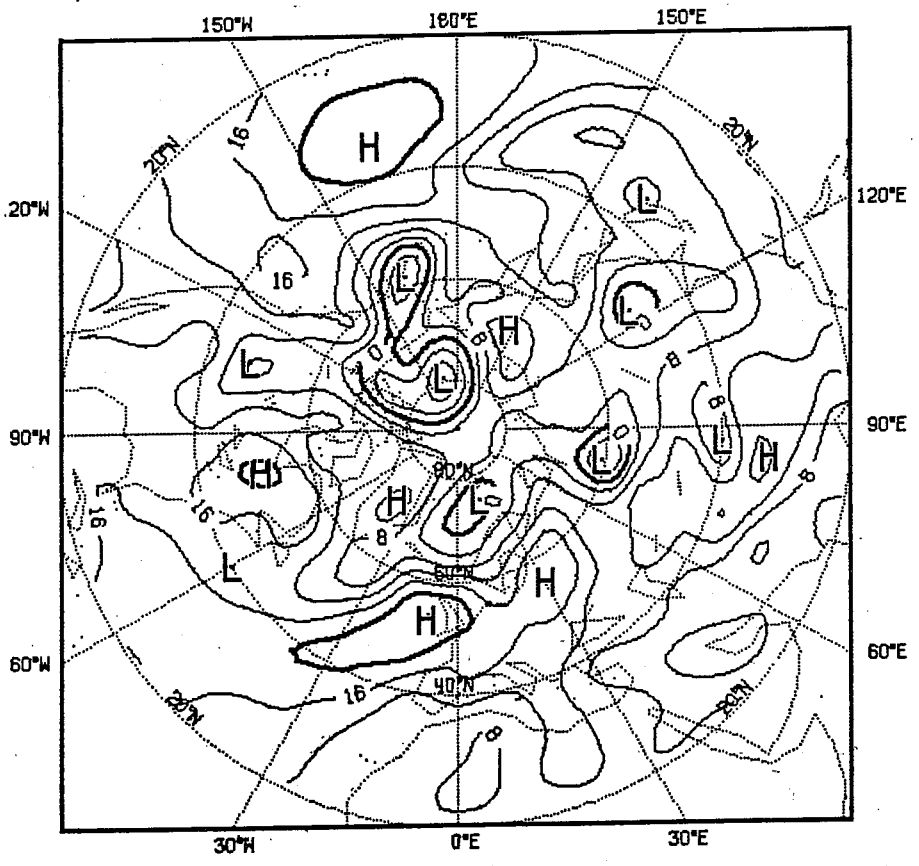

Fig. 10 (Contd.)

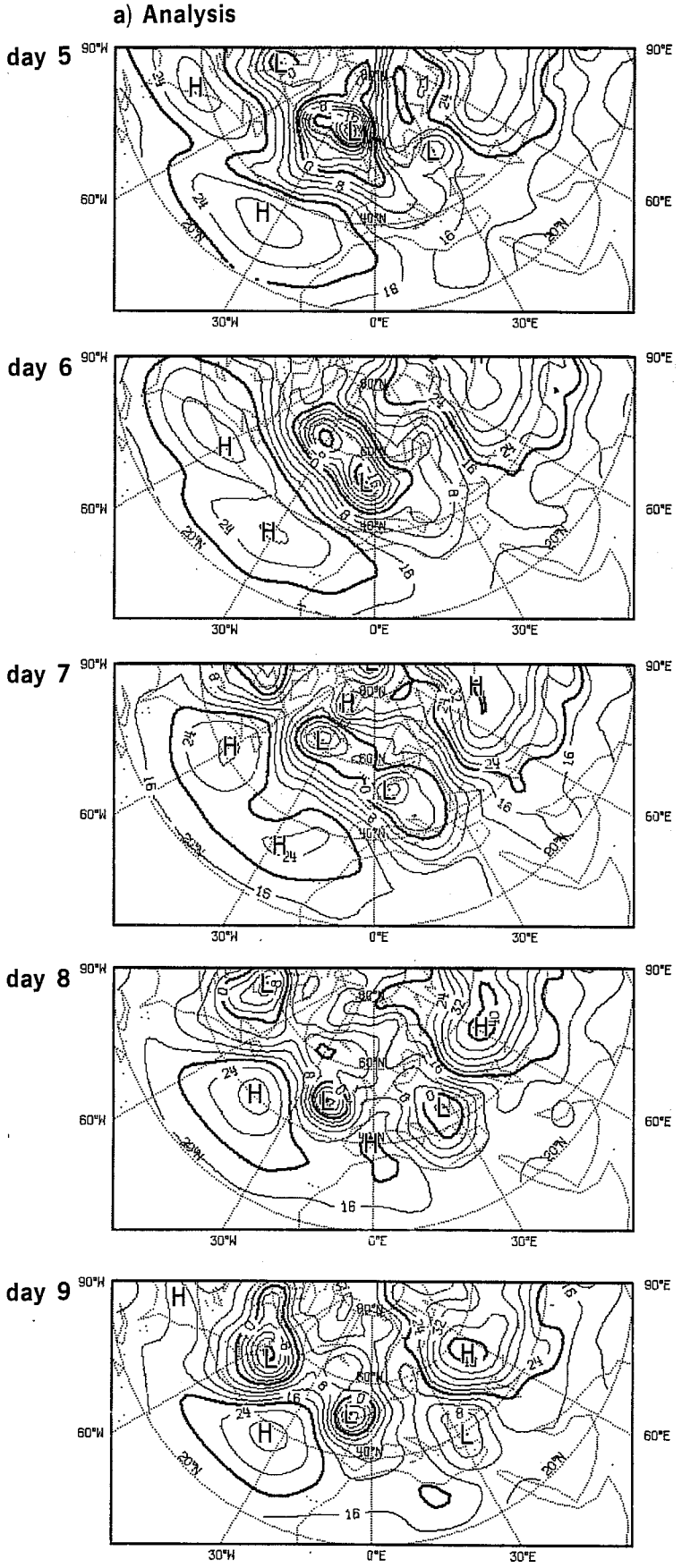

Fig. 11 Day 5-9 for forecast from 17.1.84, 1000 mb height field.
a) Analysis, b) control, c) scheme B2.

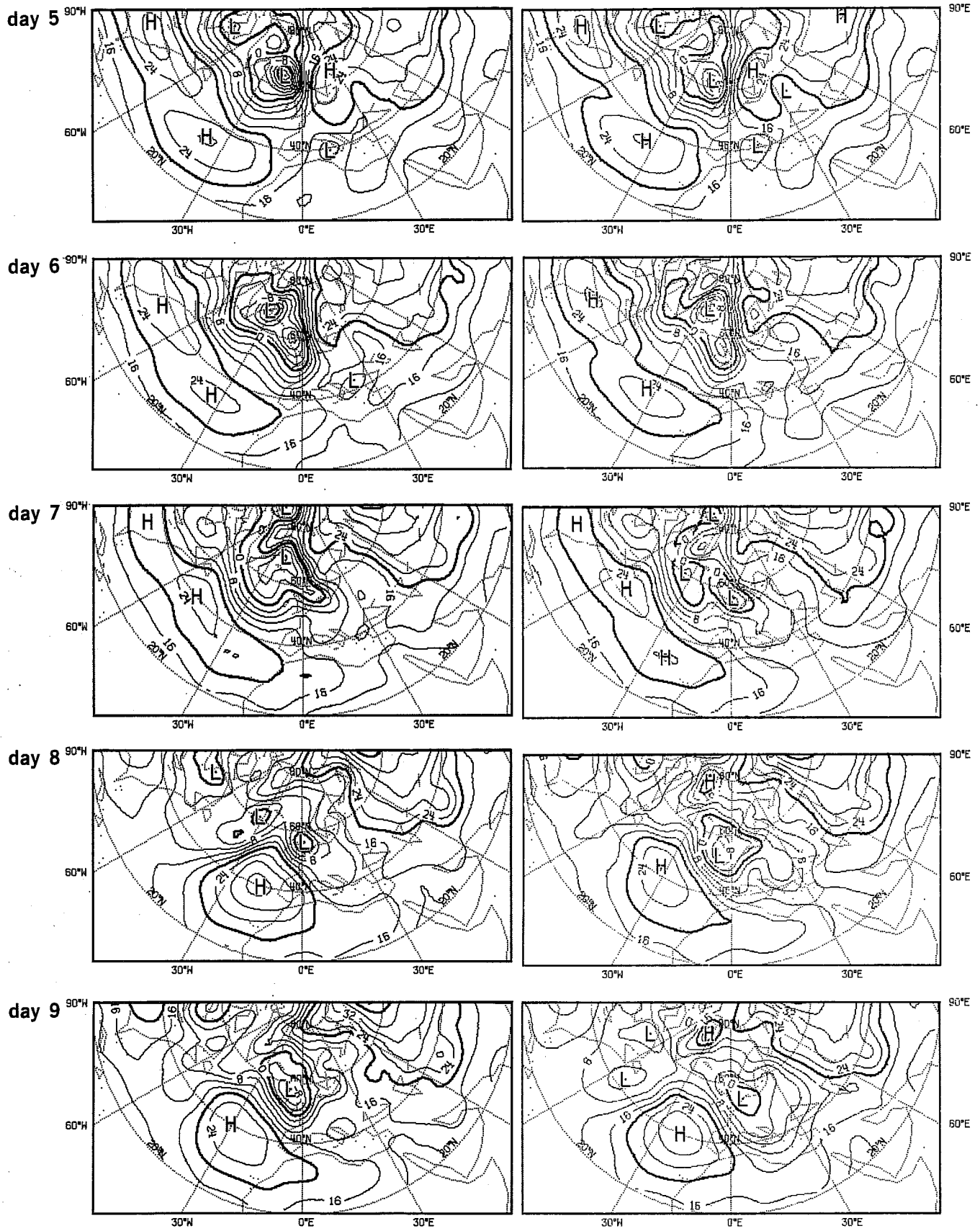
b) Control
c) Scheme B2
day 5
day 6
day 7
day 8
day 9
90°W
60°W
90°E
60°E
30°W
0°E
30°E
40°N
20°N

Fig. 11 (Contd.)

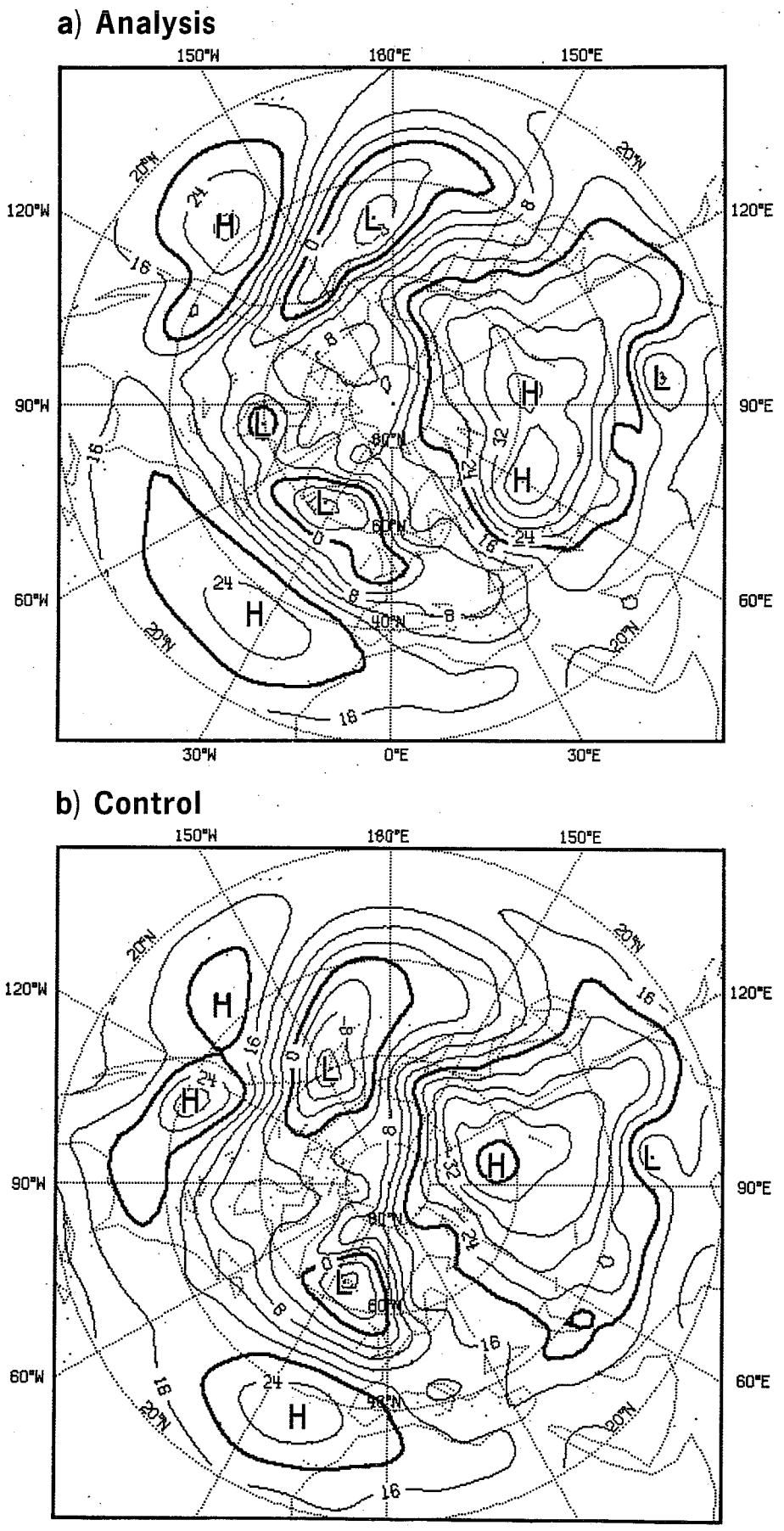

Fig. 12 Time averaged 1000 mb height field day 5-10 for T63 forecast from 17.1.84 a) Analysis, b) control, c) scheme B2

c) Scheme B2

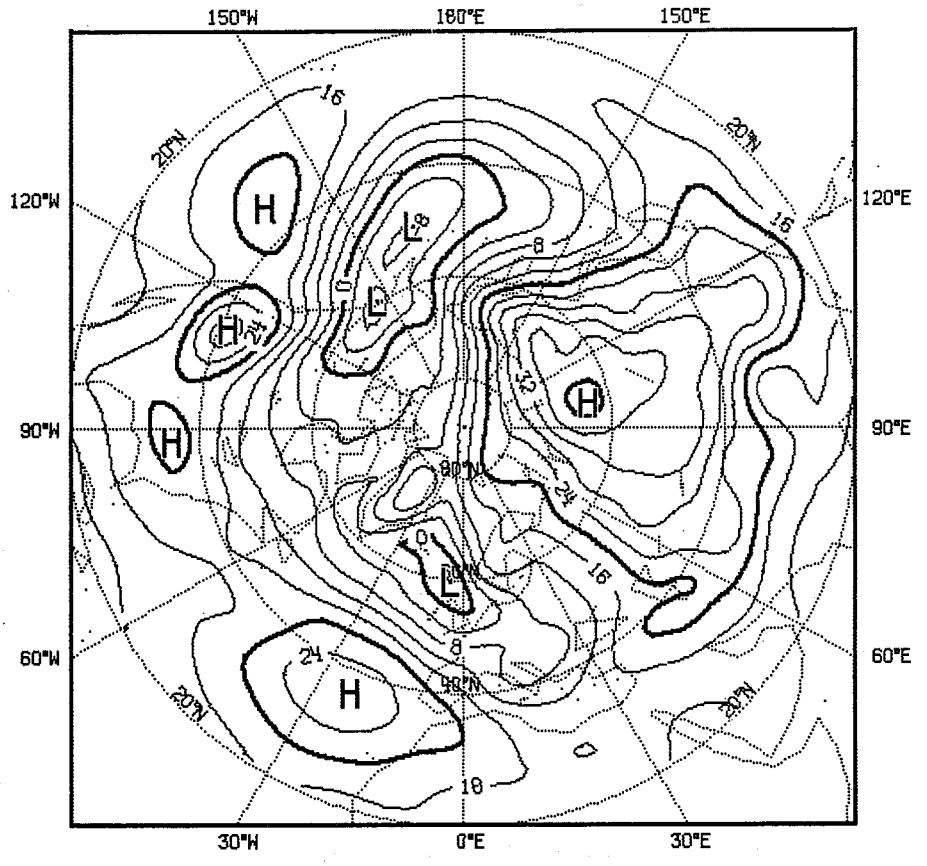

Fig. 12 (Contd.)

Fig. 9 shows 8 day forecasts of the 1000 mb height field for the control and the two finite element schemes, and the verifying analysis; the initial date was 25 February 1983. All forecasts are good with many of the major highs and lows being captured by all schemes; the anomaly correlations for this case (see case 3 in Fig. 5) remain above 60% for the whole 10 day period. With respect to the objective scores the finite element schemes did not improve on the control run for this particular case (see Fig. 5). The only difference of any significance between the forecasts is the prediction of the low at 170°W in the B2 forecast.

Fig. 10 shows day 7 forecasts from 23.8.83 for the control and scheme B2. The main difference between these is the treatment of the Atlantic low near 30°W which the B2 scheme positions more accurately.

In addition to the 6 cases listed in Table 2 a T63 forecast was run from 17.1.84; this was a period of strong cyclonic activity over the Atlantic. Fig. 11 shows the 1000 mb height field for days 5 to 9. A difference in the development of the Atlantic-European lows is noticeable at about day 7; this can also be seen in the time averaged fields (days 5 to 10). Fig. 12 shows the averaged 1000 mb height fields for days 5-10. Note that the B2 scheme gives a better representation of the elongation of the Atlantic Pacific lows.

4. 50 DAY INTEGRATIONS

50 day integrations (initial date 17 January 1984) were performed in order to investigate the influence of the different numerical schemes on the model's climate. The integrations were carried out with a T42 model. For the case chosen the objective scores are high. This is illustrated by Fig. 13 which shows the anomaly correlation and the standard deviation of height for the first 20 days of the forecast for the control run and runs with the finite element schemes B0 and B4. The B4 scheme was chosen because it evolved from the B2 scheme and avoids the problem of the noise in the top most level associated with the B2 scheme. The control run maintains a correlation over 60% up to day 10; after day 10, the finite element integrations are somewhat better.

Fig. 14 shows the time-averaged 500 mb height fields for days 25 to 50 of the finite difference control experiment, the B0 and B4 forecasts, and the verifying (mean) analysis. The main deficiencies in the control run are as follows:

- The polar vortex is too strong and incorrectly orientated.
- The troughs over the Pacific and North America are out of phase, with the model producing a ridge at 120°W where there should be a trough.
- The split of the flow at 0°E is only poorly represented by the control integration.

The finite element simulations (particularly the B4 integration) are less zonal than the control, and both have a more accurate description of the elongation of the polar vortex.

Both finite element schemes provide a better description of the troughs and ridges over North America and the Pacific; the B4 simulation being particularly good. However, only the B4 model produced a good description of the split of the flow near 0°E. It is interesting to note that the only difference between the B4 and B0 schemes is the treatment of the upper boundary condition.

Fig. 15 shows time averaged (days 26 to 50) differences of the 500 mb height fields from the climate for analyses, control run and schemes B0 and B4. The finite element integrations give the better anomaly patterns, mainly by not over developing the main two large negative anomalies in the northern hemisphere. However, since we are dealing with only one case, there may be a large sampling error involved.

The impact of the numerical treatment on the model climate is also reflected in the fluxes. Fig. 16 shows the zonally average meridional heat flux $\overline{vT}$ for days 26 to 50; the B4 finite element model giving the best results, in particular near the top level.

The strong impact of different top boundary formulations on the forecast is intriguing and it is worth investigating if similar improvements could be obtained by changing the upper boundary in the finite difference model. In this model the geopotential for full levels k is computed as:

$$\phi_k = \phi_{k+\frac{1}{2}} + \alpha_k RT_k$$

For the operational version of the model, $\alpha=\ell n2$ is used for the top level.

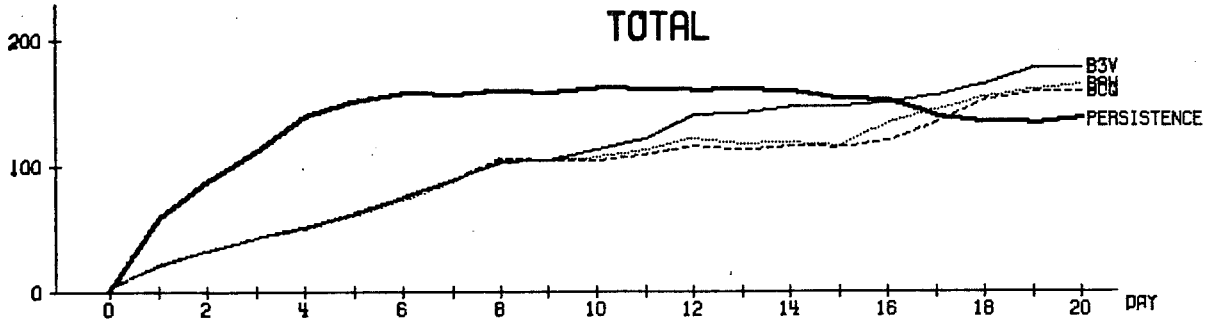

MEAN 1000- 200 MB AND 20.0 TO 82.5
ANOM-CORRELATION OF HEIGHT %

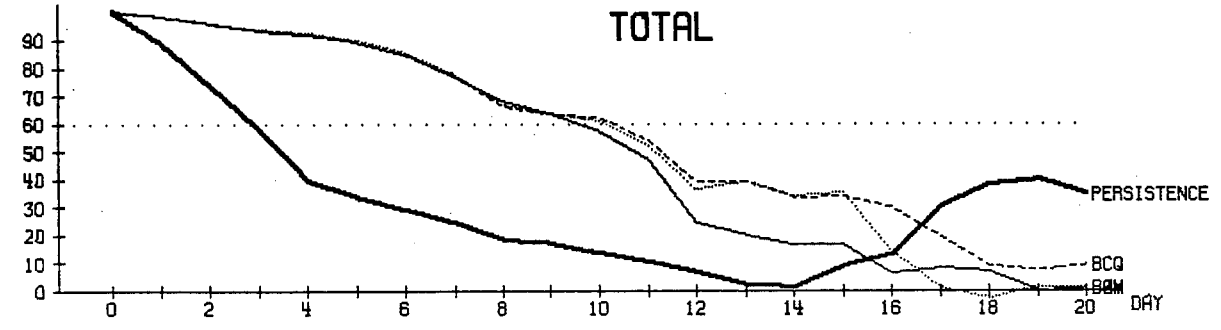

MEAN 1000- 200 MB AND 20.0 TO 82.5
STD-DEVIATION OF HEIGHT (M)

Fig. 13 Mean 1000-200 mb standard deviation and anomaly correlations of height for the forecast starting 17 January 1984 for control, schemes BO and B6, and persistence.

a) Analysis

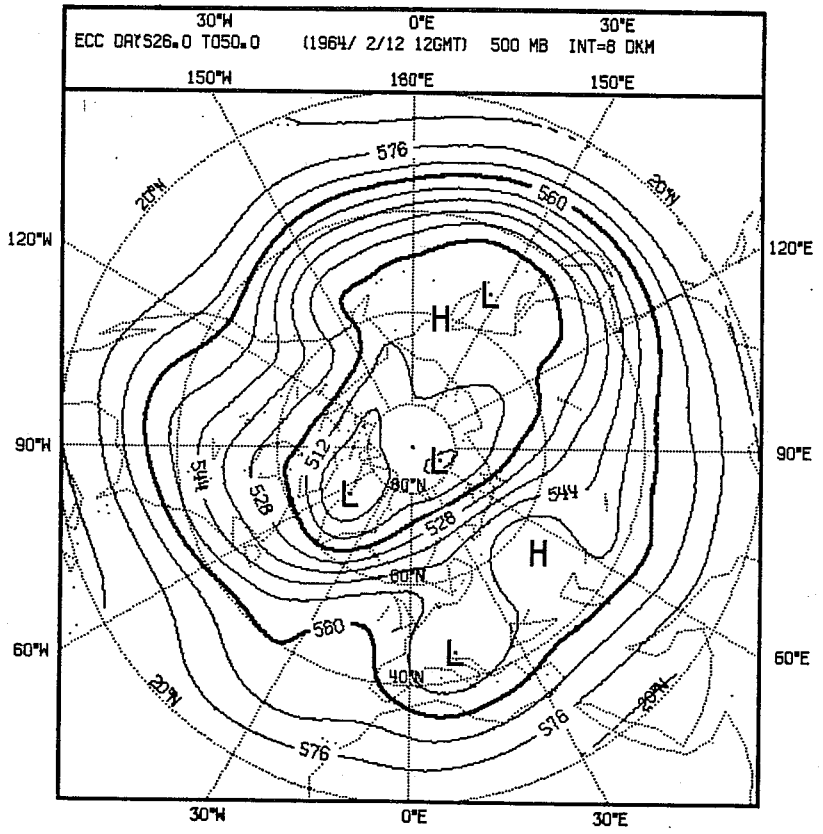

b) Control

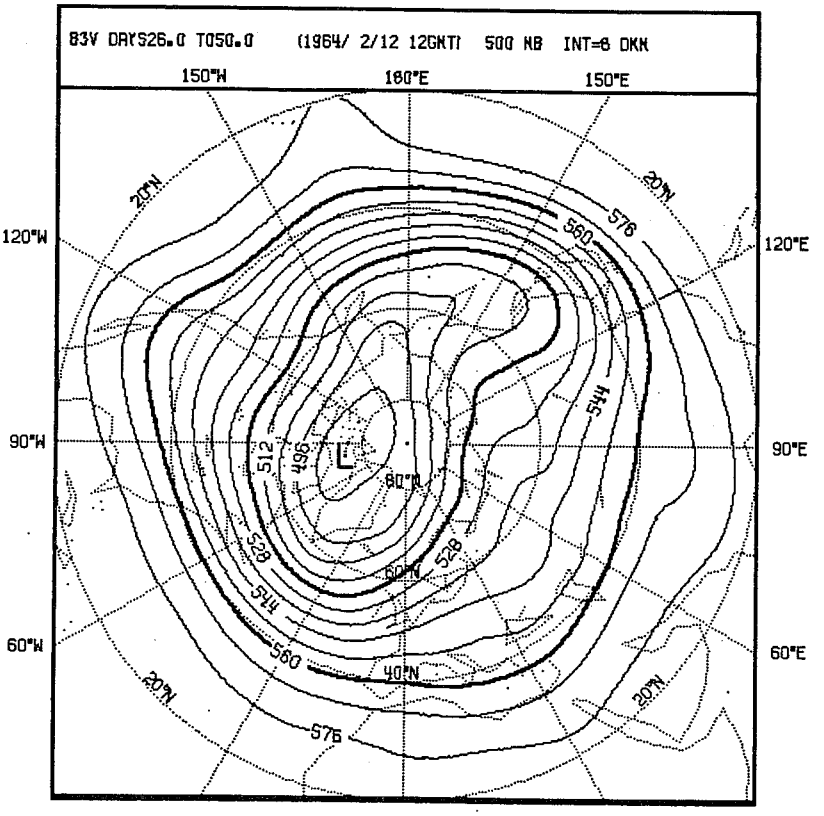

Fig. 14 500 mb height fields averaged over days 25 to 50 for (a) analysis, (b) control, (c) scheme BO and (d) scheme B4.

c) Scheme B0

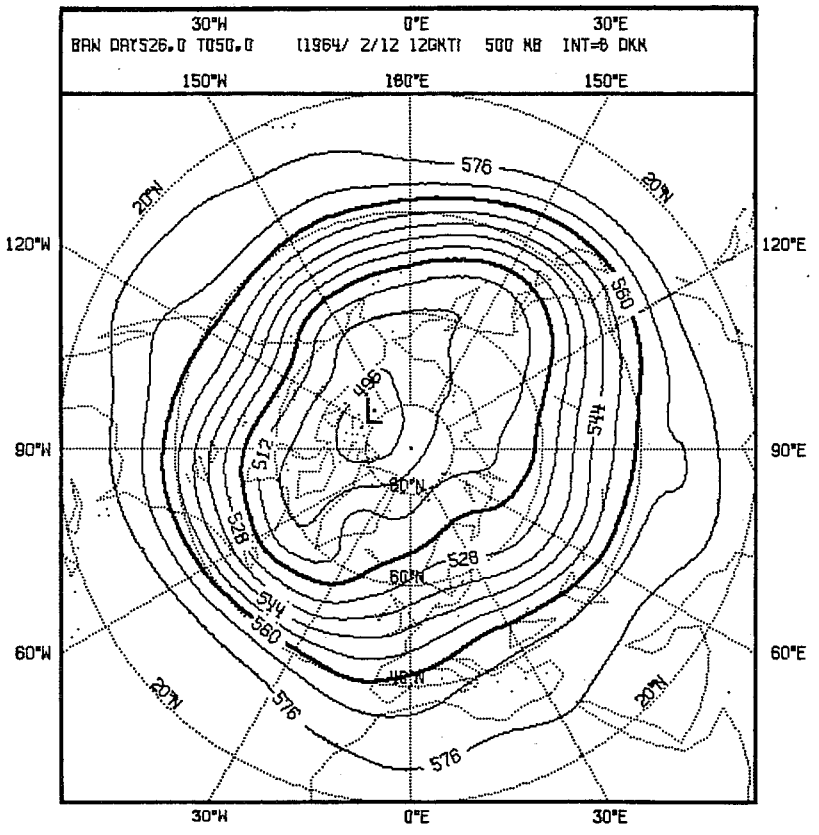

d) Scheme B4

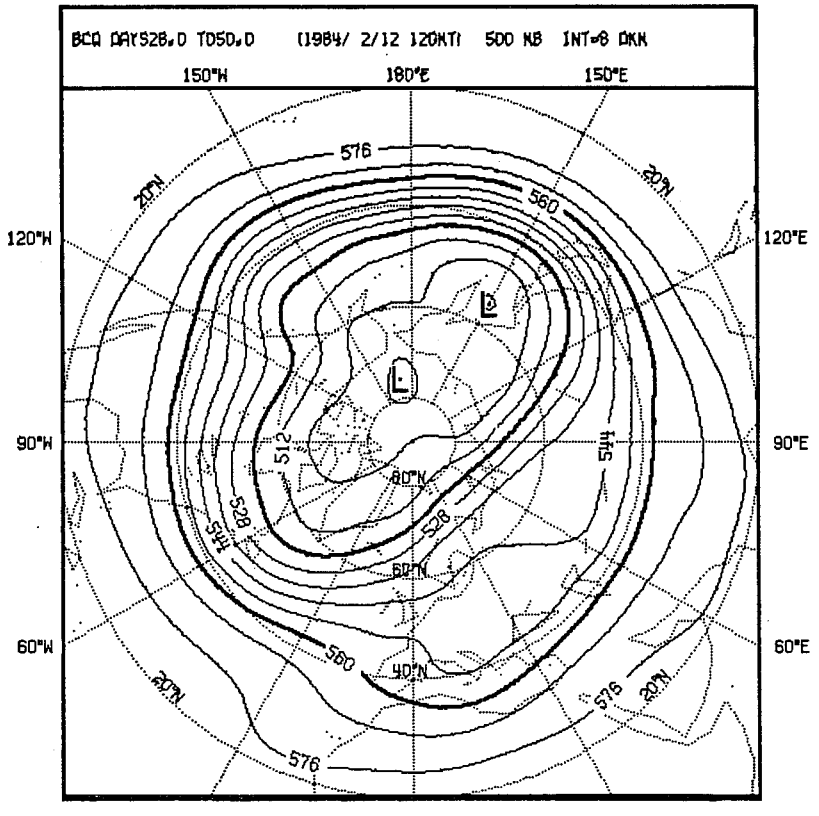

Fig. 14 (Contd.)

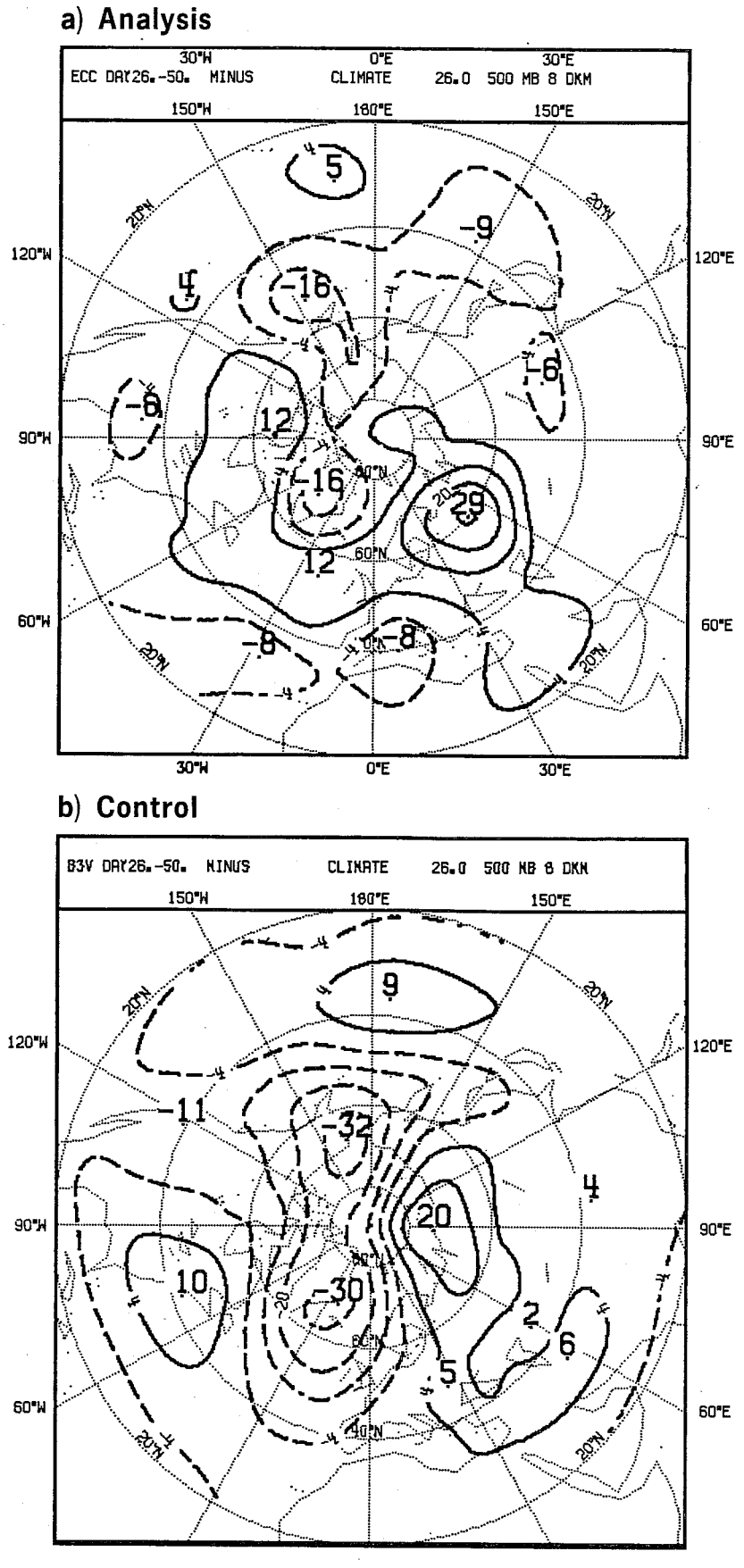

Fig. 15 As Fig. 14, but for the deviation of the 500 mb height field from the climate.

c) Scheme B0

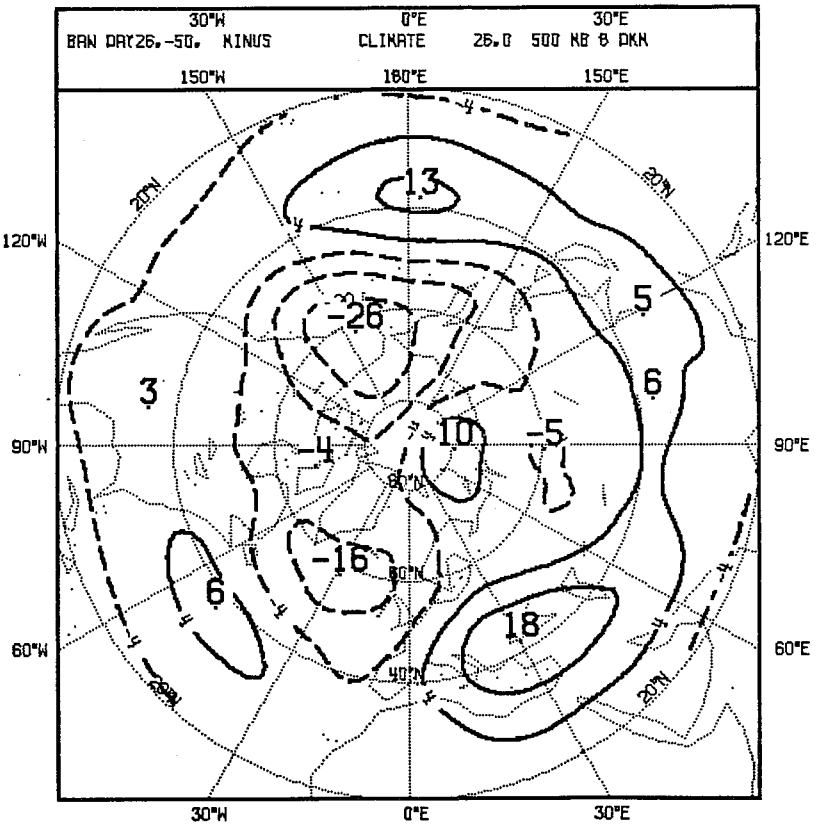

d) Scheme B4

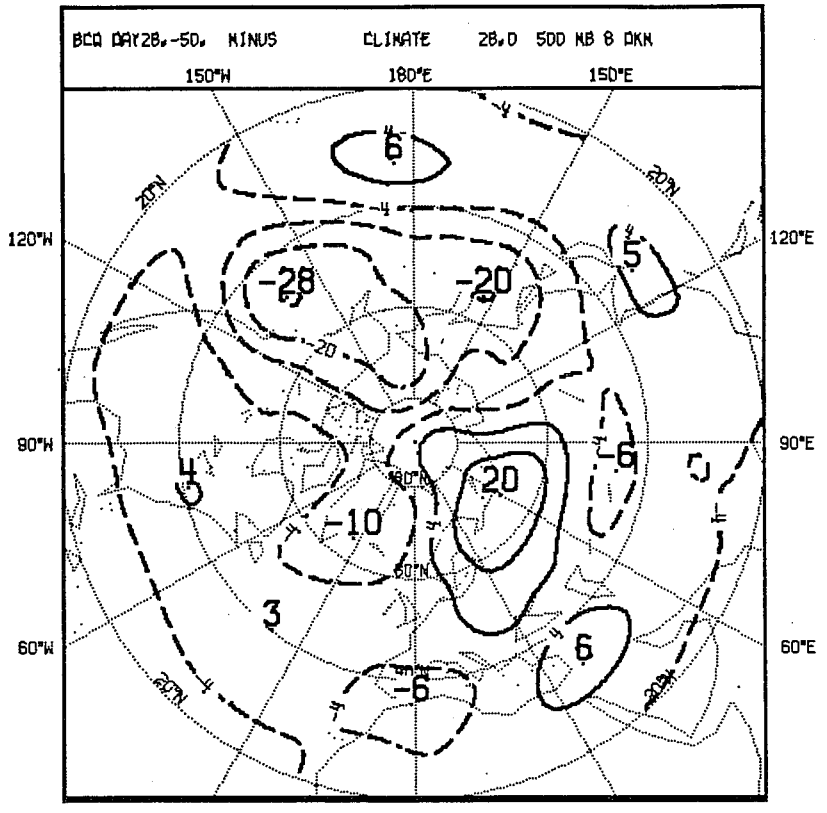

Fig. 15 (Contd.)

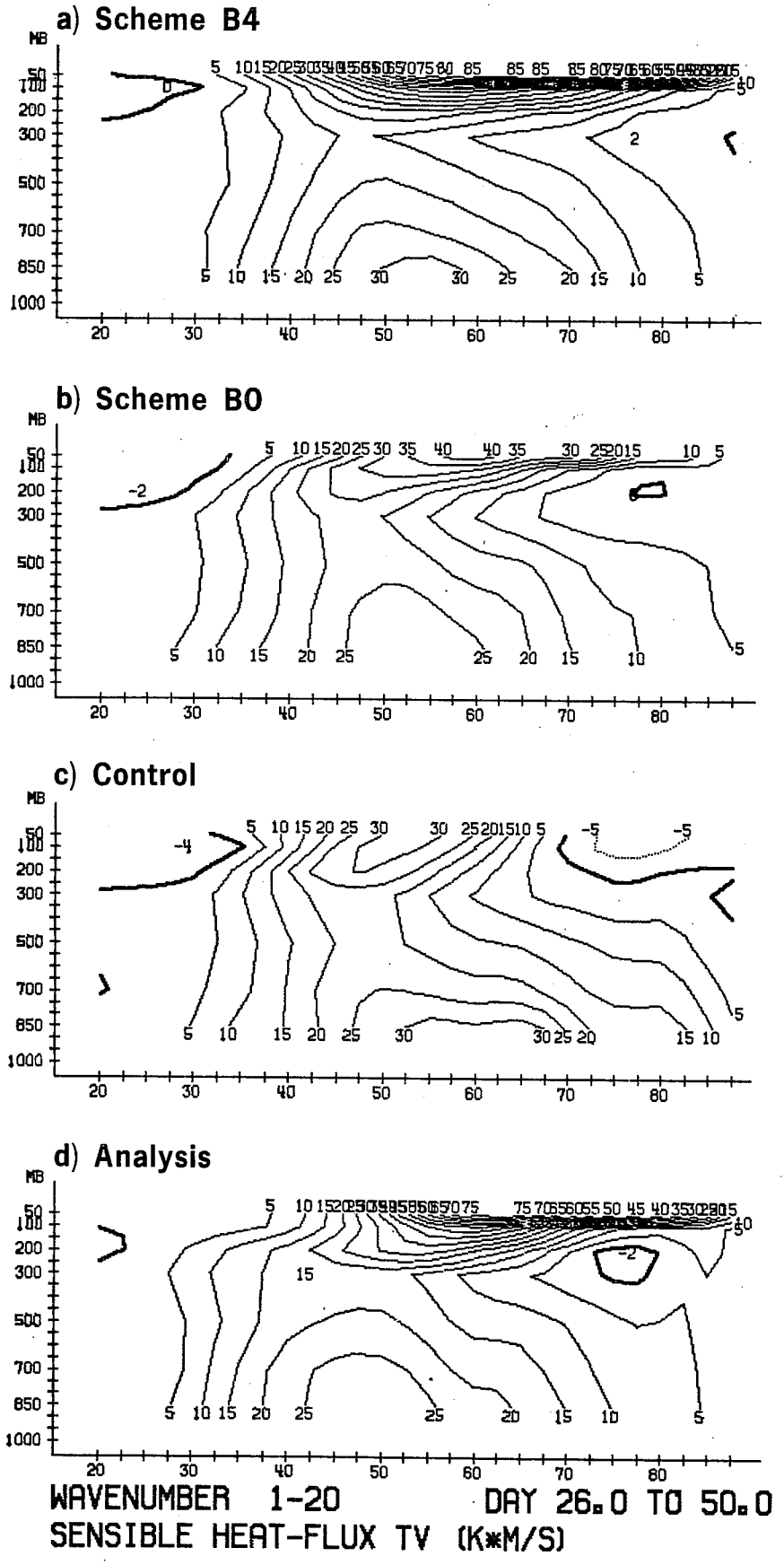

Fig. 16 Zonal average of the sensible heat flux for (a) analysis, (b) control, (c) scheme BO and (d) scheme B4.

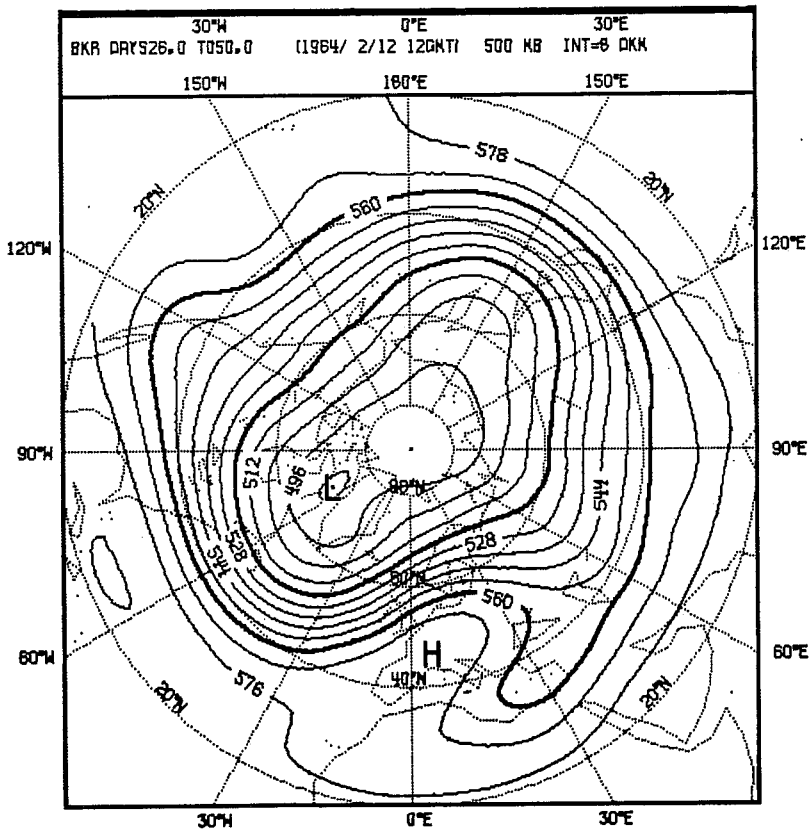

Fig. 17 As Fig. 14, but for the finite difference scheme with a modified top boundary.

The simplest way of introducing the features of finite element schemes into existing finite difference codes is to consider them as finite element schemes with piece-wise constant basis functions, as proposed in Steppeler (1982). The ECMWF operational difference scheme can be obtained as a B-scheme with piece-wise constant basis functions. The basis functions for full level k are 1 for $\sigma \in (\sigma_{k-\frac{1}{2}}, \sigma_{k+\frac{1}{2}})$, and 0 otherwise. The full level amplitudes ϕ_k are obtained as layer averages of the exactly integrated hydrostatic equation.

To obtain the B2 boundary with piece-wise constant elements, we have to assume

$$\sigma_{1/2}=0$$

$$\tilde{T} = T_1 \frac{\sigma - \sigma_{1/2}}{\sigma_{3/2}-\sigma_{1/2}} \text{ for } \sigma \in (0,\sigma_{3/2})$$

and that $\tilde{T}$ is piece-wise constant for the other levels. For ϕ_1, we obtain, with the averaging operation corresponding always to the interval $(\sigma_{1/2}, \sigma_{2/3})$

$$\phi_1 = \bar{\phi} = \phi_{3/2} - \overline{\int_{\sigma_{3/2}}^{\sigma} RT_1 \frac{\sigma - \sigma_{1/2}}{\sigma(\sigma_{3/2}-\sigma_{1/2})} d\sigma}$$

$$= \phi_{3/2} - RT_1 \overline{\frac{\sigma - \sigma_{3/2}}{(\sigma_{3/2}-\sigma_{1/2})}}$$

$$= \phi_{3/2} - \frac{RT_1}{(\sigma_{3/2}-\sigma_{1/2})^2} \int_0^{\sigma_{3/2}} (\sigma-\sigma_{3/2})\, d\sigma$$

$$= \phi_{3/2} + .5\ RT_1$$

Therefore, with $\alpha_1=0.5$, we obtain the equivalent of the B2 scheme for the ECMWF finite difference model.

Fig. 17 gives the time averaged 500 mb height field. The difference between this and the control run given in Fig. 14 is considerable. An

improvement in the shape of the polar vortex is apparent. There is also a significant difference compared to the control run in that some splitting of the flow over the Atlantic is produced and the trough at 120°W has a greater amplitude.

5. CONCLUSIONS

Several finite element schemes for vertical discretization have been implemented with the ECMWF spectral model. Two energy conserving schemes were tested on 7 cases and these resulted in a systematic improvement of the anomaly correlation of height; when compared to a single differencing technique the average increase of predictability for the two finite element schemes was 2.5 hrs (scheme B0), and 6.5 hrs (B2 scheme). In addition the use of the finite element schemes led, for a few cases, to synoptic improvements after day 7 of the forecasts.

Different specifications of the top elements had a substantial impact on the forecast, and the impact of the discretization and the different boundary formulations on the model climate appears to be substantial. 50 day integrations for one case showed that for one case finite element schemes had more skill in predicting the anomaly of the time averaged fields than a finite difference shceme.

References

Beaudoin, C. and A. Staniforth, 1980: Experiments with a model using the finite element method for vertical discretization. Research Activities in Atmospheric and Oceanic Modelling, I. Rutherford (ed), GARP Programme on Numerical Experimentation, Rep.No.21, 53-54.

Béland, M., J. Côté and A. Staniforth, 1983: The accuracy of a finite-element vertical discretization scheme for primitive equation models: comparison with a finite-difference scheme. Mon.Wea.Rev., 111, 2298-2318.

Cliffe, K.A., 1981: On conservative finite element formulations of the inviscid Boussinesq equations. Int.J.Num.Meth.Fluids, 1, 117-127.

Côté, J., M. Béland and A. Staniforth, 1983: Stability of vertical discretization schemes for semi-implicit primitive equation models: theory and application. Mon.Wea.Rev., 111, 1189-1207.

Francis, P.E., 1972: The possible use of Laguerre polynomials for representing the vertical structure of numerical models of the atmosphere. Quart.J.Roy.Meteor.Soc., 98, 662-667.

Jespersen, D.C., 1974: Arakawa's method is a finite element method. J.Computational Phys., 16, 383-390.

Machenhauer, B., and R. Daley, 1972: A baroclinic primitive equation model with a spectral representation in three dimensions. Institute of Theoretical Meteorology, University of Copenhagen, Rep.No.4, 62 pp.

Manton, M.J., 1978: A finite element model of a moist atmospheric boundary layer. Part 1: Model equations, Part 2: Method of solution, Tellus, 30, 219-220 and 229-239.

Miyakoda, K., 1982: Essay on dynamical long-range forecasts of atmospheric circulation. J.Meteor.Soc.Japan, 60, 292-308.

Simmons, A.J., and R. Strüfing, 1981: An energy and angular momentum conserving finite difference scheme, hybrid coordinates and medium-range weather prediction. ECMWF Tech.Rep.No.28, 68pp.

Staniforth, A.N., and R.W. Daley, 1977: A finite-element formulation for the vertical discretization of sigma coordinate primitive equation models. Mon.Wea.Rev., 105, 1108-1118.

Steppeler, J., 1982: Treatment of discontinuous finite element basis functions as distributions. Beitr.Phys.Atm., 55, 43-60.

APPENDIX 1

DERIVATION OF SOME EQUATIONS FOR THE A-SCHEME

a) The continuity equation

The $W_{k+\frac{1}{2}}$ of (15) are determined by the equation

$$(e_k^F, (\frac{\partial W^H}{\partial \sigma} + D)) = 0 \tag{A1}$$

The scalar product being defined in (7) together with

$$\dot{\sigma}_{\frac{1}{2}} = \dot{\sigma}_{NLEV+\frac{1}{2}} = a \tag{A2}$$

provides the right number of equations for the NLEV+2 quantities $\sigma_{\nu+\frac{1}{2}}$ and $\dot{P}_s$.

b) The ω term of the thermodynamic equation

The approximation $\dot{\sigma}_{1/2}$ for $\dot{\sigma}$ provides the ω-term of the thermodynamic equation by using

$$\omega = W^H + \sigma \underline{V}.\nabla p_s \tag{A3}$$

In (A3) W^H is given by (15) in the half-level representation. Since $\underline{V}$ is defined for full levels, the second term of (A3) is represented at full levels.

According to (17), ω is represented partly by half and full level basis functions. Using the non-discretized form of (17), and the hydrostatic equation, we obtain

$$\frac{RT}{\sigma}\omega = \frac{RT}{\sigma} W + RT\underline{v}.\nabla p_s$$

$$= - \phi_\sigma W + RT\underline{v}.\nabla p_s \tag{A4}$$

$$= - (\phi W)_\sigma + \phi\, W_\sigma + RT\nabla p_s$$

Observing that w is approximated on half levels, and using (14), we obtain

$$\frac{RT}{\sigma}\,\omega\Big|_{App} = G^F[(-\phi^H W^H)_\sigma - \phi^H D + RT\underline{v}\cdot\nabla p_s] \qquad (A5)$$

In (A5), the fields without index H are represented by full levels.

c) The vertical advection term

For the vertical advection term of temperature, we write

$$\dot{\sigma}T_\sigma = (\dot{\sigma}T)_\sigma - T\dot{\sigma}_\sigma$$

$$= (\dot{\sigma}T)_\sigma + T\left(\frac{\dot{p}_s}{p_s} + \frac{\nabla\cdot(p_s\underline{v})}{p_s}\right) \qquad (A6)$$

For (A6), we introduce the approximation

$$\dot{\sigma}T_\sigma\Big|_{App} = G^F[(\dot{\sigma}^H\,(G^H T))_\sigma + T\left(\frac{\dot{p}_s}{p_s} + \frac{\nabla\cdot(p_s\underline{v})}{p_s}\right)] \qquad (A7)$$

APPENDIX 2

PROOF OF ENERGY CONSERVATION FOR THE B-SCHEMES

To prove energy conservation, we use the vertical integrals of kinetic and potential energy, and show that the time derivative of their sum can be written as a horizontal divergence. The proof mainly uses the fact that the energy expression contains only two factors actually dependent on the vertical coordinate. It is well known that energy conservation is a property of the straightforward Galerkin method in cases where it is a second order moment of the fields (Jespersen 1974). The method of proof was for a simplified case used in Steppeler (1982).

With $K = \frac{1}{2}\,\underline{v}\cdot\underline{v}$ we obtain for the vertically integrated kinetic energy equation

$$\left(\int_0^1 p_s K d\sigma\right)^{\cdot} = \int_0^1 \dot{p}_s K d\sigma + p_s \int_0^1 \dot{K} d\sigma \tag{A8}$$

and from (25b) we obtain, using (7) for the definition of the scalar product (,),

$$\int_0^1 \dot{K} d\sigma = -(\underline{v},\ G_a \underline{\dot{v}}\cdot\nabla\underline{v} + G_a \nabla\tilde{\phi}) - (\underline{v},\ G_a \tilde{R}\tilde{T}\nabla \ell n p_s) \tag{A9}$$

We apply (12) to bring the Galerkin operations in (A8) to the other side of the scalar product. From (13) it follows that $G_a\underline{v} = \underline{v}$.

$$\int_0^1 \dot{K} d\sigma = -(\underline{v},\dot{\sigma}\underline{v}) - (\underline{v},\underline{v}\cdot\nabla\underline{v}) - (\underline{v},\nabla\phi) - (\underline{v},\tilde{R}\tilde{T}\nabla \ell n p_s) \tag{A10}$$

(A10) contains no approximating Galerkin operators G; also the first term of (A8) does not contain approximating operators because of the exact computation of $\dot{\sigma}$ and $\dot{p}_s$.

We now obtain the following when the Galerkin operations are removed from the thermodynamic equation as in (A8):

$$\left(\int_0^1 C_p p_s T\right)^{\cdot} = C_p \dot{p}_s \int_0^1 T d\sigma + C_p p_s \int_0^1 \dot{T} d\sigma \tag{A11}$$

$$C_p p_s \int_0^1 \dot{T} d\sigma = - (C_p p_s \underline{v} \cdot \nabla T) - (C_p p_s, \dot{\sigma} T_\sigma) \tag{A12}$$

$$+ (R, \frac{\tilde{T} W_1}{\sigma}) + (R, \frac{\tilde{\tilde{T}} W_2}{\sigma})$$

With all Galerkin operations removed, the usual transformations used to prove energy conservation in the continuous case can now be applied to write the time derivative of the total energy as a horizontal divergence

$$\frac{\partial}{\partial t} \int_0^1 (p_s K + \phi_s p_s + C_p p_s T)\, d\sigma$$

$$= - \nabla \cdot \left(\int_0^1 p_s \underline{v} K d\sigma\right) - \nabla \cdot \left(\int_0^1 p_s \underline{v} \tilde{\phi} d\sigma\right) - \nabla \cdot \left(\int_0^1 C_p p_s \underline{v} T d\sigma\right)$$

ECMWF PUBLISHED TECHNICAL REPORTS

No. 1 A Case Study of a Ten Day Prediction

No. 2 The Effect of Arithmetic Precisions on some Meteorological Integrations

No. 3 Mixed-Radix Fast Fourier Transforms without Reordering

No. 4 A Model for Medium-Range Weather Forecasting - Adiabatic Formulation

No. 5 A Study of some Parameterizations of Sub-Grid Processes in a Baroclinic Wave in a Two-Dimensional Model

No. 6 The ECMWF Analysis and Data Assimilation Scheme - Analysis of Mass and Wind Fields

No. 7 A Ten Day High Resolution Non-Adiabatic Spectral Integration: A Comparative Study

No. 8 On the Asymptotic Behaviour of Simple Stochastic-Dynamic Systems

No. 9 On Balance Requirements as Initial Conditions

No. 10 ECMWF Model - Parameterizationb of Sub-Grid Processes

No. 11 Normal Mode Initialization for a Multi-Level Gridpoint Model

No. 12 Data Assimilation Experiments

No. 13 Comparisons of Medium Range Forecasts made with two Parameterization Schemes

No. 14 On Initial Conditions for Non-Hydrostatic Models

NO. 15 Adiabatic Formulation and Organization of ECMWF's Spectral Model

No. 16 Model Studies of a Developing Boundary Layer over the Ocean

No. 17 The Response of a Global Barotropic Model to Forcing by Large-Scale Orography

No. 18 Confidence Limits for Verification and Energetic Studies

No. 19 A Low Order Barotropic Model on the Sphere with the Orographic and Newtonian Forcing

No. 20 A Review of the Normal Mode Initialization Method

No. 21 The Adjoint Equation Technique Applied to Meteorological Problems

No. 22 The Use of Empirical Methods for Mesoscale Pressure Forecasts

No. 23 Comparison of Medium Range Forecasts made with Models using Spectral or Finite Difference Techniques in the Horizontal

No. 24 On the Average Errors of an Ensemble of Forecasts

ECMWF PUBLISHED TECHNICAL REPORTS

No.25 On the Atmospheric Factors Affecting the Levantine Sea

No.26 Tropical Influences on Stationary Wave Motion in Middle and High Latitudes

No.27 The Energy Budgets in North America, North Atlantic and Europe Based on ECMWF Analyses and Forecasts

No.28 An Energy and Angular-Momentum Conserving Vertical Finite-Difference Scheme, Hybrid Coordinates, and Medium-Range Weather Prediction

No.29 Orographic Influences on Mediterranean Lee Cyclogenesis and European Blocking in a Global Numerical Model

No.30 Review and Re-assessment of ECNET - a Private Network with Open Architecture

No.31 An Investigation of the Impact at Middle and High Latitudes of Tropical Forecast Errors

No.32 Short and Medium Range Forecast Differences between a Spectral and Grid Point Model. An Extensive Quasi-Operational Comparison

No.33 Numerical Simulations of a Case of Blocking: the Effects of Orography and Land-Sea Contrast

No.34 The Impact of Cloud Track Wind Data on Global Analyses and Medium Range Forecasts

No.35 Energy Budget Calculations at ECMWF: Part I: Analyses

No.36 Operational Verification of ECMWF Forecast Fields and Results for 1980-1981

No.37 High Resolution Experiments with the ECMWF Model: a Case Study

No.38 The Response of the ECMWF Global Model to the El-Nino Anomaly in Extended Range Prediction Experiments

No.39 On the Parameterization of Vertical Diffusion in Large-Scale Atmospheric Models

No.40 Spectral characteristics of the ECMWF Objective Analysis System

No.41 Systematic Errors in the Baroclinic Waves of the ECMWF Model

No.42 On Long Stationary and Transient Atmospheric Waves

No.43 A New Convective Adjustment Scheme

No.44 Numerical Experiments on the Simulation of the 1979 Asian Summer Monsoon

No.45 The Effect of Mechanical Forcing on the Formation of a Mesoscale Vortex

ECMWF PUBLISHED TECHNICAL REPORTS

No.46 Cloud Prediction in the ECMWF Model

No.47 Impact of Aircraft Wind Data on ECMWF Analyses and Forecasts during the FGGE Period, 8-19 November 1979 (not on WP, text provided by Baede)

No.48 A Numerical Case Study of East Asian Coastal Cyclogenesis

No.49 A Study of the Predictability of the ECMWF Operational Forecast Model in the Tropics

No.50 On the Development of Orographic Cyclones

No.51 Climatology and Systematic Error of Rainfall Forecasts at ECMWF

No.52 Impact of Modified Physical Processes on the Tropical Simulation in the ECMWF Model

No.53 On the Performance and Systematic Errors of the ECMWF Tropical Forecasts (1982-1984)

No.54 Finite Element Schemes for the Vertical Discretization of the ECMWF Forecast Model Using Linear Elements